Context-Dependent Modification of PFKFB3 in Hematopoietic Stem Cells Promotes Anaerobic Glycolysis and Ensures Stress Hematopoiesis

Short running title: PFKFB3 supports HSC stress response

Shintaro Watanuki[1,2,†], Hiroshi Kobayashi[1,†], Yuki Sugiura[3,4,★], Masamichi Yamamoto[5], Daiki Karigane[1,2], Kohei Shiroshita[1,2], Yuriko Sorimachi[1,6], Shuhei Koide[7], Motohiko Oshima[7], Akira Nishiyama[9], Koichi Murakami[9,10], Miho Haraguchi[1], Shinpei Tamaki[1], Takehiro Yamamoto[3], Tomohiro Yabushita[8], Yosuke Tanaka[8,11], Hiroaki Honda[12], Shinichiro Okamoto[2], Nobuhito Goda[6], Tomohiko Tamura[9,10], Ayako Nakamura-Ishizu[13], Makoto Suematsu[3,14], Atsushi Iwama[7], Toshio Suda[11,15], Keiyo Takubo[1,16,★]

[1] Department of Stem Cell Biology, Research Institute, National Center for Global Health and Medicine, Tokyo 162-8655, Japan

[2] Division of Hematology, Department of Medicine, and [3] Department of Biochemistry, Keio University School of Medicine, Tokyo 160-8582, Japan

[4] Center for Cancer Immunotherapy and Immunobiology, Kyoto University Graduate School of Medicine, Kyoto 606-8501, Japan.

[5] Department of Research Promotion and Management, National Cerebral and Cardiovascular Center, Osaka 564-8565, Japan

[6] Department of Life Sciences and Medical BioScience, Waseda University School of Advanced Science and Engineering, Tokyo 162-8480, Japan

[7] Division of Stem Cell and Molecular Medicine, Center for Stem Cell Biology and Regenerative Medicine, and [8] Division of Cellular Therapy, The Institute of Medical Science, The University of Tokyo, Tokyo 108-8639, Japan

[9] Department of Immunology, Yokohama City University Graduate School of Medicine, Kanagawa 236-0004, Japan

[10] Advanced Medical Research Center, Yokohama City University, Kanagawa 236-0004, Japan

[11] International Research Center for Medical Sciences, Kumamoto University, Kumamoto 860-0811, Japan

[12] Field of Human Disease Models, Major in Advanced Life Sciences and Medicine, Institute of Laboratory Animals, and [13] Department of Microscopic and Developmental Anatomy, Tokyo Women's Medical University, Tokyo 162-8666, Japan

[14] Live Imaging Center, Central Institute for Experimental Animals, Kanagawa 210-0821, Japan

[15] Cancer Science Institute of Singapore, National University of Singapore, Singapore 117599, Singapore
[16] Japan Agency for Medical Research and Development (AMED), Core Research for Evolutional Science and Technology (CREST), Tokyo 100-0004, Japan

[†] These authors contributed equally.

★ Corresponding Authors:
Keiyo Takubo, M.D., Ph.D.
Department of Stem Cell Biology, Research Institute
National Center for Global Health and Medicine
1-21-1 Toyama, Shinjuku-ku, Tokyo 162-8655, Japan
keiyot@gmail.com / ktakubo@ri.ncgm.go.jp

Yuki Sugiura, Ph.D.
Center for Cancer Immunotherapy and Immunobiology
Kyoto University Graduate School of Medicine
Yoshida-Konoe, Sakyo-ku, Kyoto 606-8501, Japan.
yuki.sgi@gmail.com

Number of figures: 7
Number of tables: 6
Number of references: 65

Scientific category: Hematopoiesis and Stem Cells

Key Points

- Combined isotope tracing, mathematical modeling, and single cell ATP analysis enable high-resolution evaluation of blood cell metabolism.
- Under stress, HSCs quickly accelerate glycolysis to meet ATP demands and maintain hematopoiesis via context-dependent PFKFB3 activation.

Abstract

Metabolic pathways are plastic and rapidly change in response to stress or perturbation. Current metabolic profiling techniques require lysis of many cells, complicating the tracking of metabolic changes over time after stress in rare cells such as hematopoietic stem cells (HSCs). Here, we aimed to identify the key metabolic enzymes that define metabolic differences between steady-state and stress conditions in HSCs and elucidate their regulatory mechanisms. Through quantitative ^{13}C metabolic flux analysis of glucose metabolism using high-sensitivity glucose tracing and mathematical modeling, we found that HSCs activate the glycolytic rate-limiting enzyme phosphofructokinase (PFK) during proliferation and oxidative phosphorylation (OXPHOS) inhibition. Real-time measurement of adenosine triphosphate (ATP) levels in single HSCs demonstrated that proliferative stress or OXPHOS inhibition led to accelerated glycolysis via increased activity of PFKFB3, the enzyme regulating an allosteric PFK activator, within seconds to meet ATP requirements. Furthermore, varying stresses differentially activated PFKFB3 via PRMT1-dependent methylation during proliferative stress and via AMPK-dependent phosphorylation during OXPHOS inhibition. Overexpression of *Pfkfb3* induced HSC proliferation and promoted differentiated cell production, whereas inhibition or loss of *Pfkfb3* suppressed them. This study reveals the flexible and multilayered regulation of HSC metabolism to sustain hematopoiesis under stress and provides techniques to better understand the physiological metabolism of rare hematopoietic cells.

KEYWORDS

hematopoietic stem cell; stem cell metabolism; PFKFB3; quantitative metabolomics; mathematical modeling; single-cell metabolic profiling; adenosine triphosphate; glycolysis; stress hematopoiesis

Introduction

Activities governing nutrient requirements and metabolic pathways in individual cells maintain tissue homeostasis and respond to stress through metabolite production. Adenosine triphosphate (ATP), produced via cytosolic glycolysis and mitochondrial oxidative phosphorylation (OXPHOS), is the universal energy currency of all organisms; it regulates all anabolic or catabolic cellular activities[1-3]. Precise control of intracellular ATP concentrations is critical, as ATP is the rate determiner of many ATP-dependent biochemical reactions[4-9].

Hematopoietic stem cells (HSCs) are tissue stem cells at the apex of the hematopoietic hierarchy; their function is maintained throughout life by a rigorous metabolic program and a complex interplay of gene expression, epigenetic regulation, intracellular signaling, chromatin remodeling, autophagy, and environmental factors[10-14]. Conventional analyses of the metabolic programs of hematopoietic stem and progenitor cells (HSPCs) have revealed diverse differentiation potentials and cell-cycling statuses and coordinated activities that maintain hematopoiesis[15-26]. Among the HSPC fractions, HSCs possess unique cell cycle quiescence, high self-renewal and differentiation capacity in response to stimuli, and resistance to cellular stress, including reactive oxygen species and physiological aging[10,27-30]. These properties are regulated by a balance between glycolysis and mitochondrial OXPHOS, requiring biosynthesis of ATP and various macromolecules that confer resilience to stress[31]. Among the known regulators of ATP-producing pathways, glycolytic enzymes maintain HSCs and hematopoietic progenitor cells (HPCs) by regulating cellular survival and cell cycle quiescence[32-34]. Loss of mitochondrial genes in HPSCs also induces HSC differentiation defects[35-37]. Moreover, disrupting the mitochondrial complex III subunit depletes both differentiated hematopoietic cells and quiescent HSCs[21]. Although glycolysis and the tricarboxylic acid (TCA) cycle are metabolically linked, pyruvate dehydrogenase kinase activity, which can uncouple these pathways, is required to maintain HSC function[32,38].

During HSC division, cell metabolism is reprogrammed to activate fatty acid β-oxidation and purine metabolism[39-41]. Furthermore, Liang et al. reported that activated HSCs mainly rely on glycolysis as their energy source[42]. However, the mechanisms by which each ATP-producing pathway and their connections are differentially regulated between HSCs and differentiated cells at steady state, during cell cycling, or during stress remain unknown. Recently, it has been shown that deeply quiescent HSCs do not activate cell cycle under stress[43-45]. Therefore, it remains unclear whether metabolic changes such as the individual ATP-producing pathways and their interconnections occur uniformly in all HSCs, including these deeply quiescent HSCs. Furthermore,

122 the underlying hub metabolic enzyme responsible for changes in the metabolic system of HSCs
123 under stress has not been identified. HSCs are essential for cell therapy, including HSC
124 transplantation, and in order to comprehensively elucidate the metabolic systems that have attracted
125 attention as their regulatory mechanisms, recent studies have included metabolomic analyses using
126 rare cell types such as HSCs[23,46-49], as well as isotope tracer analyses of undifferentiated
127 hematopoietic cells purified after *in vivo* administration of isotopic glucose[50]. Although these
128 approaches are useful for obtaining comprehensive information on intracellular metabolites, they are
129 not suited to track real-time changes in cellular metabolism at high resolution. Therefore, new
130 approaches are necessary to analyze metabolites quantitatively and continuously without disturbing
131 the physiological states of single cells while integrating the recently reported metabolome analysis
132 techniques. In this study, we aimed to identify the key metabolic enzymes that define metabolic
133 differences between steady-state and stress conditions in HSCs and elucidate their regulatory
134 mechanisms using a quantitative and mathematical approach. Our findings provide a platform for
135 quantitative metabolic analysis of rare cells such as HSCs, characterize the overall metabolic
136 reprogramming of HSCs during stress loading, and highlight the key enzyme involved in this
137 process.
138

139 **Methods**

140 **Mice**

141 C57BL/6 mice (7–16 weeks old, Ly5.2^{+}) were purchased from Japan SLC (Shizuoka, Japan).
142 C57BL/6 mice (Ly5.1^{+}) were purchased from CLEA Japan (Shizuoka, Japan). Knock-in mice
143 harboring GO-ATeam2[51-53] in the ROSA26 locus were generated in the Yamamoto laboratory. The
144 GO-ATeam2 mice (8–16 weeks old) were used to analyze HSPCs. mVenus-p27K^{-} mice (17–20
145 weeks old) were provided by the Kitamura Laboratory at The Institute of Medical Science, The
146 University of Tokyo and used for cell cycle analysis[54,55]. Mice were genotyped using PCR-based
147 assays of tail DNA or transdermal enhanced green fluorescent protein (EGFP) fluorescence. All mice
148 were maintained in the animal facility at the National Center for Global Health and Medicine
149 Research Institute under specific pathogen-free conditions and fed ad-libitum. Mice were euthanized
150 by cervical dislocation. All animal experiments were approved by the Institutional Animal Care and
151 Use Committee (IACUC) at National Center for Global Health and Medicine Research Institute.
152 Both male and female mice were used in experiments.
153

Ion chromatography mass spectrometry (IC-MS) analysis

For metabolome analysis focused on glycolytic metabolites and nucleotides, anionic metabolites were measured using an orbitrap-type MS (Q-Exactive Focus; Thermo Fisher Scientific, Waltham, MA, USA) connected to a high-performance IC system (ICS-5000+, Thermo Fisher Scientific), enabling highly selective and sensitive metabolite quantification owing to the IC-separation and Fourier Transfer MS principle[56]. The IC instrument was equipped with an anion electrolytic suppressor (Dionex AERS 500; Thermo Fisher Scientific) to convert the potassium hydroxide gradient into pure water before the sample entered the mass spectrometer. Separation was performed using a Dionex IonPac AS11-HC-4 μm IC column (Thermo Fisher Scientific). The IC flow rate was 0.25 mL/min supplemented post-column with 0.18 mL/min makeup flow of MeOH. The potassium hydroxide gradient conditions for IC separation were as follows: 1–100 mM (0–40 min), 100 mM (40–50 min), and 1 mM (50.1–60 min), with a column temperature of 30 °C. The Q-Exactive Focus mass spectrometer was operated under ESI negative mode for all detections. Full mass scan (*m/z* 70−900) was performed at a resolution of 70,000. The automatic gain control target was set at 3×10^6 ions, and the maximum ion injection time was 100 ms. Source ionization parameters were optimized with spray voltage at 3 kV, and other parameters were as follows: transfer temperature, 320 °C; S-lens level, 50; heater temperature, 300 °C; sheath gas, 36; and aux gas, 10. Metabolite amounts were quantified from calibration curve data generated based on peak areas and respective metabolite amounts. Detailed methods for sample collection and IC-MS analysis are described in **SUPPLEMENTARY METHODS**.

Time-course analysis of ATP levels in single hematopoietic cells using GO-ATeam2 system

GO-ATeam2 is a ratiometric biosensor that monitors ATP concentration through Förster resonance energy transfer (FRET) from EGFP to the monomeric version of Kusabira Orange (mKO), regardless of the sensor expression levels[52]. Surface-marker-stained bone marrow (BM) mononuclear cells (MNCs) from GO-ATeam2 mice were dispensed into basal medium (Ba-M) containing minimal salts, vitamins, and buffers (HEPES and sodium bicarbonate), but no glucose or mitochondrial substrates (Table S1), or into medium containing mitochondrial substrates, pyruvate, lactate, fatty acids, and amino acids, but no glucose (PLFA medium). The FRET/EGFP ratio was analyzed in a real-time with a BD FACSAria IIIu Cell Sorter (BD Biosciences, Franklin Lakes, NJ, USA) under ambient pressure, and ATP levels were calculated. Detailed methods for sample collection and ATP concentration calculation are provided in **SUPPLEMENTARY METHODS**.

186

187 **Statistical analysis**

188 Data are presented as means ± SD, unless otherwise stated. For multiple comparisons, statistical
189 significance was determined by Tukey's multiple comparison test using the Tukey HSD function in R
190 ×64 4.0.3 software (R Core Team, Vienna, Austria). A paired or unpaired two-tailed Student's *t*-test
191 and two-way ANOVA with Sidak's test were used for experiments with two groups. A p-value <0.05
192 was considered statistically significant.

193

194 **Data sharing**

195 All relevant data are available from the corresponding author upon reasonable request.

196

197 **Results**

198 **HSC cell cycling increases anaerobic glycolytic flux**

199 To determine how cell cycle progression alters HSC metabolism *in vivo*, we intraperitoneally and
200 intravenously treated mice with 5-fluorouracil (5-FU) to induce HSC cell cycling (Supplemental
201 Figure 1A). For analysis after 5-FU administration, the Lineage (Lin)$^-$ Sca-1$^+$ c-Kit$^+$ (LSK) gate was
202 expanded to include as many HSCs as possible, for example high Sca-1-expressing cells and c-Kit-
203 high to -dim Lin$^-$ cells, based on the previous report[57] (Supplemental Figure 1B). This expanded LSK
204 gate was consistent with the patterns of Sca-1 and c-Kit expression observed in EPCR$^+$ Lin$^-$ CD150$^+$
205 CD48$^-$ cells, and the presence of EPCR, as a surface marker, identified HSCs with high stem cell
206 activity after 5-FU administration[41]. We observed a transient decrease in the number of quiescent
207 HSCs (Ki67$^-$) and an increase in the number of cell-cycling HSCs (Ki67$^+$) on day 6 after 5-FU
208 treatment (Supplemental Figure 1C). Along with the loss of cell quiescence, ATP concentration in
209 HSCs decreased transiently on day 6 (Supplemental Figure 1D). Because the route of administration
210 of 5-FU (intraperitoneal or intravenous) made no difference in the Ki67 positivity rate of HSCs
211 (Supplemental Figure 1E), we administered 5-FU intraperitoneally for remaining experiments. Two
212 other methods were used to test whether cell cycle progression of HSCs after 5-FU treatment
213 depends on the expression of EPCR. First, phosphorylation of Rb (pRb), a marker of cell cycle
214 progression[58], was analyzed in HSCs after 5-FU treatment. Analysis of EPCR$^+$ and EPCR$^-$ HSCs
215 showed increased pRb in HSCs from 5-FU-treated mice in both fractions compared to HSCs from
216 phosphate-buffered saline (PBS)-treated mice, regardless of EPCR expression (Supplemental Figure
217 1F-G). Second, we used a G_0 marker mouse line[55]. These mice expressed a fusion protein of the p27

218 inactivation mutant p27K$^-$ and the fluorescent protein mVenus (G_0 marker), allowing prospective
219 identification of G_0 cells. We tested whether the expression of G_0 marker in HSCs was altered after
220 5-FU administration to the G_0 marker mice (Supplemental Figure 1H) and found that 5-FU treatment
221 reduced the frequency of G_0 marker-positive HSCs, regardless of the EPCR expression
222 (Supplemental Figure 1I-J). This was not observed in the PBS group. These results indicated that 5-
223 FU administration induced cell cycle progression of entire HSCs in mice.

224 HSC cell cycling is preceded by the activation of intracellular ATP-related pathways that
225 metabolize extracellular nutrients, including glucose[39,40], which are utilized in both ATP-producing
226 and -consuming pathways, determining cellular ATP levels. Therefore, we examined the metabolic
227 flux of glucose by performing *in vitro* IC-MS tracer analysis with uniformly carbon-labeled (U-$^{13}C_6$)
228 glucose to determine the pathways driving changes in ATP in 5-FU-treated HSCs (Figure 1A; Table
229 S2). To avoid metabolite changes, samples were continuously chilled on ice during cell preparation,
230 and the process from euthanasia to cell preparation was performed in the shortest possible time (see
231 "**Preparation and storage of in vitro U-$^{13}C_6$-glucose tracer samples**" section under
232 "**Supplementary Methods**" for more information). We found that changes in metabolite levels
233 before and after sorting were present but limited (Supplemental Figure 2A). This result is consistent
234 with the finding that the cell purification process does not significantly affect metabolite levels when
235 sufficient care is taken in cell preparation[50]. In 5-FU-treated HSCs, the levels of glycolytic
236 metabolites derived from U-$^{13}C_6$-glucose were double those observed in PBS-treated HSCs (Figure
237 1B-C; Supplemental Figure 2B). The total levels of TCA cycle intermediates derived from U-$^{13}C_6$-
238 glucose were similar between PBS- and 5-FU-treated cells (Figure 1D; Supplemental Figure 2B).
239 Levels of U-$^{13}C_6$-glucose-derived intermediates involved in the pentose phosphate pathway (PPP)
240 and nucleic acid synthesis (NAS) were two-fold higher in 5-FU-treated than in PBS-treated HSCs,
241 whereas no significant differences in the levels of metabolites were observed between both groups
242 (Figure 1E-F; Supplemental Figure 2B). Notably, the labeling rate of metabolites during the first half
243 of glycolysis was almost 100% in both groups, allowing us to easily track the labeled metabolites
244 (Supplemental Figure 2C-E). This was thought to be due to the rapid replacement of unlabeled
245 metabolites with labeled metabolites during exposure to U-$^{13}C_6$-glucose because of the generally
246 rapid glycolytic reaction. Next, we evaluated whether glucose uptake in HSCs after 5-FU
247 administration was differentially affected by the expression of EPCR. The fluorescent analog of
248 glucose, 2-(N-(7-nitrobenz-2-oxa-1,3-diazol-4-yl)amino)-2-deoxyglucose (2-NBDG), was
249 administered intravenously to mice[50] and its uptake in EPCR$^+$ and EPCR$^-$ HSCs was assayed (Figure

1G). Regardless of the EPCR expression, the 2-NBDG uptake was greater in HSCs treated with 5-FU than in those treated with PBS (Figure 1H-J). Furthermore, compared with HSCs cultured under quiescence-maintaining conditions, those cultured under proliferative conditions were more resistant to OXPHOS inhibition by oligomycin (Supplemental Figure 1H; Table S1). Overall, the results showed that 5-FU-treated HSCs exhibited activated glycolytic flux, increasing the turnover of ATP. Moreover, glycolytic flux into mitochondria was equally unchanged in PBS- and 5-FU-treated-HSCs, supporting that 5-FU activated anaerobic glycolysis in HSCs.

OXPHOS-inhibited HSCs exhibit compensatory glycolytic flux

Previous studies using mouse models of mitochondrial disease or defects in genes involved in electron transport chain and OXPHOS suggest that mitochondrial energy production is essential for maintaining HSC function[21,35-37], as is the glycolytic system. However, there have been no quantitative reports on how OXPHOS-inhibited HSCs can adapt their metabolism. To understand HSC metabolism under OXPHOS inhibition, we performed *in vitro* U-$^{13}C_6$-glucose tracer analysis of oligomycin-treated HSCs (Figure 2A; Table S3). Similar to 5-FU-treated HSCs (Figure 1), oligomycin-treated HSCs exhibited glycolytic system activation (Figure 2B-C; Supplemental Figure 2B). Metabolite flux to the TCA cycle and PPP was unchanged, but flux to the NAS was significantly reduced in oligomycin-treated HSCs compared to that in steady-state HSCs (Figure 2D-F; Supplemental Figure 2B). The results suggested that OXPHOS-inhibited HSCs activated compensatory glycolytic flux and suppressed NAS flux. As with 5-FU-treated HSCs, analysis of oligomycin-treated HSCs also showed almost 100% labeling of metabolites in the first half of glycolysis (Supplemental Figure 2F-H), allowing us to easily track the labeled metabolites. To further validate the compensatory glycolytic activation of HSCs under OXPHOS inhibition, a Mito Stress test was performed on HSCs and other differentiated myeloid progenitors (MyPs, Lin$^-$Sca-1$^-$c-Kit$^+$ (LKS$^-$) cells). The results showed that extracellular acidification rates (ECAR) were elevated in HSCs after oligomycin treatment compared to before oligomycin treatment (Figure 2G-H). No increase in ECAR was observed in MyPs (Figure 2G-H), supporting that inhibition of OXPHOS activated anaerobic glycolysis specifically in HSCs.

Phosphofructokinase (PFK) metabolism in HSCs is activated during proliferation and OXPHOS inhibition

To investigate whether glycolytic activation in HSCs after 5-FU treatment and OXPHOS inhibition

282 could be demonstrated through unbiased mathematical simulations, we performed quantitative ^{13}C
283 metabolic flux analysis (^{13}C-MFA). After generating a metabolic model for isotope labeling
284 enrichment and setting appropriate lactate efflux values, a simulation was conducted using the
285 labeled metabolite abundance data obtained from isotope tracer analysis. The appropriate lactate
286 efflux for quiescent HSC (PBS-treated HSC) was determined to 65 after experimenting with values
287 from 0–100. The lactate efflux of 5-FU- or oligomycin-treated HSCs was higher than that of
288 quiescent HSCs based on the observation that labeled glycolytic metabolite levels were particularly
289 elevated in *in vitro* tracer analysis (see "**Quantitative ^{13}C-MFA with OpenMebius**" under
290 "**Supplementary Methods**" for more information). As a result, the variation in the flux values of all
291 enzymatic reactions calculated in HSCs after 5-FU or oligomycin treatment became smaller
292 compared to quiescent HSCs, suggesting that HSCs strictly regulated their metabolism in response to
293 stress (Supplemental Figure 3A-C). Unlike PBS-treated HSCs, those treated with 5-FU or
294 oligomycin exhibited preferential glycolytic activation rather than TCA- or PPP-based metabolic
295 strategies; the first half of the glycolytic system appeared to be the site of metabolic activation
296 (Figure 3A-D; Supplemental Figure 3D-U, Table S4). This increase in metabolic flux upstream of the
297 glycolytic pathway was also supported by our *in vitr*o tracer analysis (Figure 1B and Figure 2B),
298 suggesting that ^{13}C-MFA was a valid metabolic simulation. Among the reactions in the first half of
299 glycolysis, phosphorylation of fructose 6-phosphate by PFK is the irreversible and rate-limiting
300 reaction[59]. A detailed review of *in vitro* isotope tracer analysis results showed that the ratio of
301 fructose 1,6-bisphosphate (F1,6BP; the product of PFK) to F6P (the substrate of PFK) was greatly
302 elevated in HSCs during proliferation and OXPHOS inhibition (Figure 3J-K). Together with the
303 results of quantitative ^{13}C-MFA, these findings suggested that HSCs exhibit elevated glycolytic flux
304 relative to mitochondrial activity by increasing PFK enzyme activity under various stress conditions.
305

306 **HSCs under stress exhibit activation of glycolysis-initiated TCA cycle and NAS**

307 To investigate the long-term glucose utilization of HSCs, we performed an *in vivo* tracer analysis
308 with U-$^{13}C_6$ glucose based on recent reports[47,50] (Supplemental Figure 4A; see "**Preparation and**
309 **storage of in vivo U-$^{13}C_6$-glucose tracer samples**" under "**Supplementary Methods**" for more
310 information). In HSCs from 5-FU-treated mice, we observed increased labeling of glycolytic
311 metabolites such as dihydroxyacetone phosphate, glycerol-3-phosphate, and phosphoenolpyruvate, as
312 well as NAS metabolites such as inosine monophosphate and ATP, and those derived from TCA
313 cycle such as aspartic acid and glutamate, compared to HSCs from PBS-treated mice (Supplemental

Figure 4B-I, Table S5). When the amount of U-$^{13}C_6$-glucose-derived labeled metabolites in each pathway was calculated, more glucose-derived metabolites entered TCA cycle in the 5-FU-treated group than PBS-treated group (Supplemental Figure 4J). Thus, although short-term (10–30 min) *in vitro* tracer analysis showed that HSCs exhibited more potent activation of anaerobic glycolysis than of other pathways in response to 5-FU administration, long-term (approx. 3 h) labeling by *in vivo* tracer analysis revealed that glycolysis-initiated TCA cycle and NAS flux were activated in addition to enhanced anaerobic glycolysis.

PFKFB3 accelerates glycolytic ATP production during HSC cell cycling

In vitro and *in vivo* tracer analysis results collectively suggested that the activation of glycolysis catalyzed by PFK may have been the starting point for the activation of the entire HSC metabolism. To analyze the contribution of PFK to ATP metabolism in steady-state or stressed HSCs, we needed to develop an experimental system that could measure the dynamics of ATP concentrations in HSCs in a non-destructive, real-time manner. To this end, we used knock-in GO-ATeam2 mice as a FRET-based biosensor of ATP concentration (see "**Time-course analysis of ATP levels in single hematopoietic cells using GO-ATeam2 system**" under "**Methods**" for more information.). The number of BMMNCs, as well as the frequency of HSCs (CD150$^+$CD48-LSK) and other progenitor cells, in the BM of GO-ATeam2$^+$ mice were almost unchanged compared to of C57B6/J mice, except for a mild decrease in the frequency of the Lin$^-$ fraction (Supplementary Figure 5A-C). Using BMMNCs derived from GO-ATeam2$^+$ mice, we developed a method to detect changes in ATP concentration with high temporal resolution when the activity of PFK was modulated (**METHODS**, Supplemental Figure 5D-F). To validate our methods, we measured ATP concentrations in HSCs and MyPs with or without various nutrients (see "**Time-course analysis of FRET values**" under "**Supplementary Methods**" for more information.). MyPs showed more rapid decreases in ATP concentration than HSCs, suggesting higher ATP consumption by progenitors (Supplemental Figure 5G-H). Adding glucose to the medium suppressed this decrease in MyPs; however, other metabolites (e.g., pyruvate, lactate, and fatty acids) had minimal effects, suggesting that ATP levels are glycolysis-dependent in MyPs (Supplemental Figure 5G-H), consistent with previous reports that the aerobic glycolytic enzyme M2 pyruvate kinase isoform (PKM2) is required for progenitor cell function[33].

Further, we analyzed ATP consumption and metabolic dependency of cell-cycling HSCs after 5-FU administration (Figure 4A). After inhibiting glycolysis using 2-deoxy-D-glucose (2-DG)

346 with other mitochondrial substrates, 5-FU-treated HSCs showed more rapid decreases in ATP
347 concentration than PBS-treated HSCs (Figure 4B-C). In contrast, OXPHOS inhibition by oligomycin
348 without glucose or mitochondrial substrates decreased the ATP concentration to a similar extent in
349 both 5-FU- and PBS-treated HSCs, although 5-FU-treated HSCs showed earlier ATP exhaustion
350 (Figure 4D-E). These data suggest that 5-FU-treated-HSCs upregulated ATP production via
351 glycolysis, rather than relying on mitochondria. Apoptosis assay revealed a slight increase in early
352 apoptotic cells (annexin V^+ propidium iodide $[PI]^-$) after 2-DG treatment and a slight decrease in the
353 number of viable cells (Annexin V^- PI^-) after oligomycin treatment, both to a very limited extent
354 (approx. 5%) compared to the degree of ATP decrease, suggesting that the decrease in ATP after 2-
355 DG or oligomycin treatment did not simply reflect cell death (Supplementary Figure 5I).
356 PFK is allosterically activated by 6-phosphofructo-2-kinase/fructose-2,6-bisphosphatase
357 (PFKFB). Among the four isozymes of mammalian PFKFB, PFKFB3 is the most favorable for PFK
358 activation[60]. We investigated whether PFKFB3 contributes to glycolytic plasticity in HSCs during
359 proliferation. When treated with the PFKFB3 inhibitor AZ PFKFB3 26, compared with HSCs from
360 PBS-treated mice, HSCs from 5-FU-treated mice showed decreased ATP levels (Figure 4F, H,
361 Supplementary Figure 5J). Although AMPK activates PFKFB3 in other contexts[61], AMPK inhibition
362 by dorsomorphin did not alter ATP concentration in 5-FU-treated-HSCs (Figure 4G, I).
363

364 **OXPHOS inhibition accelerates glycolysis to sustain ATP levels in HSCs, but not in progenitors**
365 To assess differences in metabolic dependence between steady-state or stressed and naturally
366 proliferating HPCs, we altered ATP metabolism in HSCs and progenitors using 2-DG or oligomycin
367 (Figure 5A). Oligomycin treatment rapidly depleted ATP in HSCs and all HPC fractions (green lines
368 in Figure 5B-C; Supplemental Figure 6A-D). Treatment with 2-DG decreased ATP concentrations for
369 a short amount of time (~12 min) in HSCs and HPCs, but ATP reduction was less evident than that
370 induced by oligomycin (blue lines in Figure 5B-C; Supplemental Figure 6A-D). The ATP reduction
371 induced by 2-DG treatment was particularly low (~15%) in HSCs, multipotent progenitor cells
372 (MPPs), and common lymphoid progenitors (CLPs) relative to that in common myeloid progenitors
373 (CMPs), granulocytes-macrophage progenitors (GMPs), and megakaryocyte-erythrocyte progenitors
374 (MEPs) (Figure 5D).
375 Next, we investigated the role of glycolysis in ATP production during OXPHOS inhibition
376 by combining oligomycin administration and glucose supplementation. ATP concentration remained
377 more stable in HSCs treated with oligomycin and glucose than in those treated only with oligomycin.

Similar results were not seen in HPCs, indicating that HSCs have the plasticity to upregulate glycolytic ATP production to meet demands (orange lines in Figure 5B-C; Supplemental Figure 6A-D, summarized in Figure 5E). Similar to oligomycin treatment, rotenone (Complex I inhibitor) and carbonyl cyanide 4-(trifluoromethoxy)phenylhydrazone (FCCP, mitochondrial uncoupler) treatments, which inhibit OXPHOS-derived ATP production, also decreased ATP concentrations in HSCs, but not when administered simultaneously with glucose (Supplementary Figure 6E-F). Furthermore, with oligomycin, HSCs, but not HPCs, maintained ATP concentrations at low glucose levels (50 mg/dL) (Supplemental Figure 6G). These analyses suggest that ATP was produced by mitochondrial OXPHOS in steady-state HSCs, and that only HSCs, but not HPCs, maintained ATP production by glycolysis when OXPHOS was compromised.

PFKFB3 accelerates glycolytic ATP production during OXPHOS inhibition

Next, to understand whether PFKFB3 contributes to ATP production in HSCs under OXPHOS inhibition, we evaluated PFKFB3 function under OXPHOS inhibition using the GO-ATeam2^{+} BMMNCs. In oligomycin-treated HSCs, PFKFB3 inhibition led to rapidly decreased ATP concentration that was not observed in HSCs not treated with oligomycin (Figure 5F-I). We examined the effects of HSPC metabolic regulators on ATP levels in oligomycin-treated HSCs. Inhibiting PKM2, which accelerates glycolysis in steady-state progenitors[33], significantly reduced ATP levels in oligomycin-treated HSCs (Supplemental Figure 6H, J). Inhibiting LKB1, a kinase upstream of AMPK[62,63], did not affect the ATP concentration in oligomycin-treated HSCs (Supplemental Figure 6I, K), whereas levels of adenosine monophosphate (AMP), which also activates AMPK, increased in oligomycin-treated but not in 5-FU-treated HSCs (Supplemental Figure 6L). This may explain differences in AMPK-dependent ATP production between proliferative HSCs and HSCs under OXPHOS inhibition.

Next, we tested the effects of PFKFB3 on ATP concentration in HPCs. Unlike HSCs, HPCs exhibited PFKFB3-dependent ATP production, even without oligomycin (Supplemental Figure 6M-Q). Therefore, ATP production in steady-state HSCs was PFKFB3-independent, and proliferative stimulation or OXPHOS inhibition plastically activated glycolytic ATP production in a PFKFB3-dependent manner to meet ATP demand.

PFKFB3 activity renders HSCs dependent on glycolysis

Next, we investigated whether PFKFB3 activity itself confers glycolytic dependence on HSCs. We

410 retrovirally overexpressed *Pfkfb3* in HSCs and performed cell cycle analysis (Figure 5J). *Pfkfb3*-
411 overexpressed HSCs increased the proportion of cells in the S/G2/M phase and decreased the number
412 of G_0 cells compared to *mock*-overexpressed HSCs (Figure 5K). Next, we retrovirally overexpressed
413 *Pfkfb3* in GO-ATeam2$^+$ HSCs and performed real-time ATP measurement (Figure 5J). *Pfkfb3*-
414 overexpressing GO-ATeam2$^+$ HSCs did not show changes in ATP concentrations relative to those in
415 *mock*-transduced cells (Figure 5L; Supplemental Figure 6R). Upon 2-DG treatment, *Pfkfb3*-
416 overexpressing HSCs showed a greater decrease in ATP concentration than *mock*-transduced HSCs
417 did (Figure 5M; Supplemental Figure 6S). However, oligomycin treatment of both *mock*-transduced
418 and *Pfkfb3*-overexpressing HSCs decreased ATP concentration to comparable levels (Figure 5N;
419 Supplemental Figure 6T). Notably, *Pfkfb3*-overexpressing HSCs recovered ATP levels more
420 effectively under low glucose conditions (12.5 mg/dL) than did *mock*-transduced HSCs (Figure 5O;
421 Supplemental Figure 6U). These data suggest that PFKFB3 directly conferred glycolytic dependence
422 onto HSCs by modulating the cell cycle and increasing their ATP-generating capacity via glycolysis
423 under metabolic stress.
424

425 **PFKFB3 methylation by PRMT1 supports ATP production by cell-cycling HSCs**

426 Next, we investigated how 5-FU-treated-HSCs regulate PFKFB3 independently of AMPK (Figure
427 4G, I). PFKFB3 activity is regulated at multiple levels[64], and PFKFB3 transcript and protein levels in
428 HSCs remained unchanged during 5-FU-induced cell cycling (Figure 6A-B). Phosphorylation can
429 also regulate PFKFB3 activity[61,65,66]; however, we observed no change in PFKFB3 phosphorylation
430 in 5-FU-treated-HSCs (Figure 6C). Upon oligomycin exposure, PFKFB3 was phosphorylated by
431 AMPK in the HSCs (Figure 6D). PFKFB3 is also methylated, and its activity is upregulated by
432 protein arginine methyltransferase 1 (PRMT1)[67]. We observed that *Prmt1* expression increased in 5-
433 FU-treated-HSCs relative to that in PBS-treated-HSCs (Figure 6E). Furthermore, PFKFB3
434 methylation was significantly induced in 5-FU-treated-HSCs than in PBS-treated-HSCs (Figure 6F).
435 Treatment of HSCs with a PRMT1 inhibitor decreased PFKFB3 methylation (Figure 6G), suggesting
436 that PRMT1 catalyzed PFKFB3 methylation. To investigate whether glycolytic activity in HSCs was
437 regulated by m-PFKFB3, mice treated with PBS or 5-FU were injected with 2-NBDG, and m-
438 PFKFB3 levels in HSCs with high and low 2-NBDG uptake were quantified. Regardless of PBS or
439 5-FU treatment, HSCs with high 2-NBDG uptake exhibited higher m-PFKFB3 levels than those with
440 low uptake (Figure 6H), suggesting that m-PFKFB3 regulated the activity of the glycolytic system in
441 HSCs.

Further, we analyzed the potential effects of PRMT1 inhibition on ATP concentration in GO-ATeam2^{+} HSCs. Treatment with the PRMT1 inhibitor significantly decreased ATP levels in 5-FU-treated-HSCs than in PBS-treated-HSCs (Figure 6I-J). These findings indicated that ATP levels in 5-FU-treated-HSCs were supported by PRMT1 methylation–mediated PFKFB3 activation.

PFKFB3 contributes to HSPC pool expansion and stress hematopoiesis maintenance

Finally, we analyzed PFKFB3 function in HSCs during hematopoiesis. We cultured HSCs with a PFKFB3 inhibitor *in vitro* under quiescence-maintaining or proliferative conditions (Supplementary Figure 7A)[68]. Cell count in HSC-derived colonies decreased following treatment with a PFKFB3 inhibitor under proliferative, but not quiescence-maintaining, conditions (Supplementary Figure 7B).

We also knocked out *Pfkfb3* in HSCs using the less toxic, vector-free CRISPR-Cas9 system and cultured the cells under quiescence-maintaining or proliferative conditions (Supplementary Figure 7A) based on recent reports by Shiroshita et al.[69]. Again, cell numbers in *Pfkfb3*-knockout (KO) HSC–derived colonies decreased only in proliferative cultures when compared to control cultures (*Rosa26*-KO HSCs) (Supplementary Figure 7C, E, F). We retrovirally overexpressed *Pfkfb3* in HSCs and cultured them under quiescence maintenance or proliferative conditions (Supplementary Figure 7A). *Pfkfb3*-overexpressing HSC colonies showed increased cell count compared to that of *mock*-transduced cells, but only under proliferative conditions (Supplementary Figure 7D).

To assess PFKFB3 function in HSCs *in vivo*, we transplanted *Pfkfb3*-KO HSCs (Ly5.2^{+}) or wild type (WT) control HSCs into lethally irradiated recipients (Ly5.1^{+}) as well as Ly5.1^{+} competitor cells (Figure 7A), and the behavior of *Pfkfb3*-KO cells was evaluated by Sanger sequencing of peripheral blood (PB) cells[69]. In the KO group, donor-derived chimerism in PB cells decreased relative to that in the WT control group during the early phase (1 month post-transplant) but recovered thereafter (Figure 7B). Next, we retrovirally transduced Ly5.2^{+} HSCs with *Pfkfb3* S461E (*Pfkfb3*CA), a constitutively active PFKFB3 mutant, and transplanted them into lethally irradiated recipients (Ly5.2^{+}), along with Ly5.1^{+} competitor cells (Figure 7A, Supplementary Figure 7G). Donor chimerism during the early post-transplant period in the *Pfkfb3*CA-overexpressing group was significantly higher than that in the *mock*-transduced group (Figure 7C). These findings suggested that PFKFB3 was required for differentiation and proliferation of HSCs to expand the HSPC pool. Therefore, we compared the contribution of PFKFB3 to HSPC function at steady state and after myeloproliferative stimulation. *Pfkfb3*- or *Rosa*-KO HSPCs were transplanted into recipients (Ly5.1^{+}). After 2 months, recipients received 5-FU intraperitoneally, and the dynamics of *Pfkfb3*- or

474 *Rosa*-KO cell abundance in PB was assessed (Figure 7D). In PB cells prior to 5-FU administration,
475 *Pfkfb3*- or *Rosa*-KO HSPC-derived blood cells were almost equally present, suggesting that the loss
476 of PFKFB3 did not affect steady-state blood cell production (Figure 7E). However, after 5-FU
477 administration, *Pfkfb3*-KO HSPC-derived blood cell abundance was reduced compared to that in the
478 *Rosa* group (Figure 7E). This change occurred on day 6 after 5-FU administration (day 1), when the
479 cell cycle of HSCs was activated (Supplementary Figure 1B), suggesting that PFKFB3 served a
480 function in the proliferation and differentiation of HSPCs from HSCs.

481 To investigate the mechanisms underlying the short-term effects of PFKFB3 on
482 hematopoiesis after bone marrow transplantation (BMT), we evaluated cell cycle and apoptosis of
483 *Pfkfb3*-KO or -overexpressing HSPCs on day 2 after BMT (Figure 7F). Cell cycle was analyzed by
484 Ki67/Hoechst33432 staining and *in vivo* BrdU labeling [50], which showed that cell cycle progression
485 was suppressed in *Pfkfb3*-KO HSPCs (Figure 7G-J). In contrast, *Pfkfb3* KO cells did not exhibit
486 aberrant apoptosis of HSPCs after BMT (Figure 7K). Furthermore, we examined the cell cycle of
487 HSPCs overexpressing *Pfkfb3*CA on day 2 after BMT (Figure 7L) and found that *Pfkfb3*CA-
488 overexpressing HSPCs showed accelerated cell cycle compared to *mock*-overexpressing HSPCs
489 (Figure 7M-N). These data indicate that PFKFB3 governs cell cycle progression and promotes the
490 production of differentiated cells from HSCs in proliferative environments, both *in vitro* in the
491 presence of cytokine stimulation and immediately after transplantation *in vivo*.

492

493 **Discussion**

494 In this study, by combining metabolomic tracing of U-$^{13}C_6$-labeled glucose and ^{13}C-MFA, we
495 quantitatively identified the metabolic programs used by HSCs during steady-state, cell-cycling, and
496 OXPHOS inhibition. Under proliferative stress, HSCs uniformly shift from mitochondrial respiration
497 to glycolytic ATP production and PPP activation, which represent hallmarks of cell-cycling
498 mammalian cells[70]. Previous reports have emphasized the importance of glycolysis in maintaining
499 HSC quiescence, but have primarily analyzed HSCs in transplant assays, wherein HSCs must enter
500 the cell cycle[32,71]. Prior analysis of repopulation capacity, which is positively correlated with
501 enhanced glycolysis, may have overestimated glycolytic ATP production and overlooked
502 mitochondrial ATP production during native hematopoiesis. In fact, some studies have suggested that
503 OXPHOS activity is important for HSC maintenance and function[21].

504 Our method was based on recently reported quantitative metabolic analysis techniques for

very small numbers of cells[23,46-50], such as HSCs, and expands our knowledge of HSC metabolism during stress hematopoiesis. In our study, 5-FU administration in mice transiently decreased ATP concentration in HSCs in parallel with cell cycle progression, suggesting that HSC differentiation and cell cycle progression are closely related to intracellular metabolism and can be monitored by measuring ATP concentration. We mainly analyzed a mixture of $EPCR^+$ and $EPCR^-$ HSCs, and we believe that the observed cell cycle progression and promotion of glycolysis in both $EPCR^+$ and $EPCR^-$ HSCs support the validity of our claims (Figure 1J, Supplementary Figure 1F-J). According to ^{13}C-MFA enzymatic reaction flux of PFK in 5-FU-treated HSCs indicated a relative increase of approximately 10%. However, the flux value obtained by ^{13}C-MFA was calculated with glucose uptake as 100. Thus, when combined with the overall increase in the glycolytic pool demonstrated by *in vitro* isotopic glucose tracer analysis and *in vivo* NBDG analysis, rapid acceleration of glycolysis becomes evident throughout the HSCs, including subpopulations that were less responsive to stress[43-45]. These findings are consistent with reports suggesting that HSCs have relatively low biosynthetic activity[72,73] that is rapidly activated in response to cell proliferation stimuli[40,74]. Notably, we found that HSCs could accelerate glycolytic ATP production to fully compensate for mitochondrial ATP production under OXPHOS inhibition, a phenomenon that is difficult to identify without real-time ATP analysis. On the other hand, we observed that ATP production in steady-state or cell-cycling HSCs and in naturally proliferating HPCs depended more on mitochondrial OXPHOS than on glycolysis; inhibiting glycolysis in steady-state HSCs resulted in only mild ATP decreases. This is in contrast with the rapid decrease in ATP levels caused by OXPHOS inhibition. Because fatty acid β-oxidation is necessary for HSC self-renewal and quiescence[39,68], fatty acids may support mitochondrial ATP production independently of fluxes from glycolysis. Furthermore, although glycolysis and TCA cycle are decoupled in steady-state HSCs, in response to cell cycle progression, anaerobic glycolytic metabolism in HSCs is enhanced (Figure 1) and fluxes to TCA cycle and PPP from the glycolytic system are also promoted (Supplementary Figure 4). The difference in the degree of coupling between glycolysis and the TCA cycle between *in vitro* and *in vivo* tracer analysis may be explained by the difference in labeling time (10–30 min vs. 3 h). Altogether, these data provide direct evidence that glycolysis and TCA cycle become functionally uncoupled in quiescent HSCs[32,38]. Our findings are also consistent with previous reports of OXPHOS activation associated with HSC proliferation[32,36,75,76]. In other words, HSCs exhibit an increased proportion of anaerobic glycolysis–derived ATP by PFKFB3 upon proliferation and OXPHOS inhibition; furthermore, the glycolytic system is the starting point of metabolic activation and is indispensable for the overall enhancement

537 of HSC metabolism (Figure 7H).

538 HPCs and leukemic cells accelerate glycolytic ATP production using PKM2 for
539 differentiation and transformation, respectively[33]; however, we demonstrated that glycolytic
540 acceleration does not fully compensate for mitochondrial ATP production in HPCs. Mechanistically,
541 PFKFB3 increased glycolytic activity in HSCs to maintain ATP concentrations during proliferation
542 and OXPHOS inhibition. Under steady-state conditions, naturally proliferating HPCs rely on
543 PFKFB3 for ATP production, whereas HSCs do not. Therefore, we can infer that quiescent HSCs at
544 steady state can produce ATP via PFKFB3 activation in response to stress, enabling ATP generation.
545 Furthermore, overexpression of *Pfkfb3* in HSCs increased glycolytic dependency, suggesting that
546 PFKFB3 itself can modulate metabolic dependency in HSCs. Changes in glycolytic dependency in
547 HSCs overexpressing *Pfkfb3* may seem small (0.06–0.13 mM) (Figure 5M, O). However, it is
548 noteworthy that the rate of the reaction catalyzed by PFK varies greatly within a very narrow range
549 of ATP concentrations, less than 1 mM. Webb et al. analyzed the factors controlling PFK activity and
550 reported that the reaction rate of PFK varies by approximately 40% in the 0.3–1 mM ATP
551 concentration range[77]. The reason that differences in glycolytic dependence could be detected in cells
552 overexpressing *Pfkfb3* may be that the ATP concentration at the time of analysis was approximately
553 0.5–0.6 mM, which is within the range where a small change in ATP concentration can dynamically
554 alter PFK activity.

555 PFKFB3 supports hematopoiesis in contexts that require robust HSPC proliferation *in vitro*
556 and *in vivo*. We showed that the positive or negative effect of *Pfkfb3* overexpression or KO on
557 differentiated blood cell production is gradually lost after BMT. This is because HSPCs require
558 PFKFB3 for cell cycle progression during stress hematopoiesis in the early phase after BMT (Figure
559 7F-J, and L-N). However, HSCs no longer require PFKFB3 for a certain period of time after BMT,
560 probably because they regain a quiescent state. This is consistent with the fact that inhibition of
561 PFKFB3 in quiescent HSCs does not reduce the ATP concentration (Figure 5F, H), suggesting that
562 the activity of PFKFB3 is plastically modified. HSC metabolic plasticity is also illustrated by the
563 mode of PFKFB3 activation, differing depending on stress type. During proliferative stress, PRMT1
564 methylates PFKFB3 in the HSCs to promote glycolytic ATP production, a modification that increases
565 its activity[67]. PRMT1 is required for stress hematopoiesis[78], but its downstream targets in HSCs
566 remain unclear. Our results strongly suggest that PRMT1 targets PFKFB3 to stimulate glycolysis in
567 HSCs. In contrast, under OXPHOS inhibition, PFKFB3 phosphorylation by AMPK is induced—
568 another modification that also upregulates its activity. These two PFKFB3 protein modifications

allow for flexible regulation of ATP production by glycolysis, even under simultaneous and different stresses. In fact, the constitutively active S461E PFKFB3 mutant, designed to mimic phosphorylation in response to OXPHOS inhibition, enhanced HSC reconstitution capacity after transplantation, suggesting that even if PFKFB3 is activated by one stress (in this case, proliferative), it has the activation capacity to respond to a different stress (i.e., mitochondrial). Therefore, the functions of phosphorylated and methylated forms of PFKFB3 are to some extent interchangeable, and either modification can be used to handle diverse stresses.

In summary, we found that HSCs exhibit a highly dynamic range of glycolytic flux. Our study highlights glycolysis as a pivotal source of energy production in stressed HSCs, and indicates that OXPHOS, although an important source of ATP, can be uncoupled from glycolysis in steady-state HSCs without compromising ATP levels. Because multiple PFKFB3 modifications safeguard HSCs against different stresses by accelerating glycolysis, interventions targeting these might effectively induce or manage stress hematopoiesis. This study provides a platform for comprehensive and quantitative real-time analysis of ATP concentration and its dynamics in HSPCs. Our approach allows for analysis of metabolic programs in rare cells and detection of various metabolic activities within a diverse cell population, making it applicable to the analysis of various tissue systems in normal and diseased states.

Acknowledgments

We thank E. Lamar for preparation of the manuscript, T. Kitamura for providing mVenus-p27K- mice, and N. Toyama-Sorimachi and H. Shindou for their critical reading of the manuscript. This work was supported in part by KAKENHI grants from MEXT/JSPS (JP19K17847 to H.K.; JP19K17877, JP21J01690 to D.K.; JP18H02845, JP20K21621, JP21H02957 to K.T.), AMED grants (JP22zf0127007 to M.S.; JP18ck0106444, JP18ae0201014, JP20bm0704042, JP20gm1210011 to K.T.), grants from the National Center for Global Health and Medicine (29-1015, 20A1010 to H.K.; 26-001, 21A2001 to K.T.), the Takeda Science Foundation (to D.K. and K.T.), a JB Research Grant (to D.K.), the Human Biology Microbiome Quantum Research Center (WPI-Bio2Q) supported by MEXT (to M.S.), and the MEXT Joint Usage/Research Center Program at the Advanced Medical Research Center, Yokohama City University (to K.T.).

Author Contributions

S.W., H.K., Y. Sugiura, M.Y., K.S., Y. Sorimachi, D.K., S.K., M.O., A.N., K.M., M.H., and S.T.

performed the study and analyzed data; T. Yamamoto, T. Yabushita, Y.T, H.H., S.O., N.G., T.T., A.N-I., M.S., A.I., T.S., and K.T. provided scientific advice and materials; S.W., H. K., A.N-I. and K.T. wrote the manuscript; and K.T. conceived the project and supervised the research.

Conflict of interest

The authors declare no competing financial interests.

References

1. Schirmer T, Evans PR. Structural basis of the allosteric behaviour of phosphofructokinase. *Nature*. 1990;343(6254):140-145.
2. Denton RM, Randle PJ, Bridges BJ, et al. Regulation of mammalian pyruvate dehydrogenase. *Mol Cell Biochem*. 1975;9(1):27-53.
3. Harris RA, Hawes JW, Popov KM, et al. Studies on the regulation of the mitochondrial alpha-ketoacid dehydrogenase complexes and their kinases. *Adv Enzyme Regul*. 1997;37:271-293.
4. Sols A. Multimodulation of enzyme activity. *Curr Top Cell Regul*. 1981;19:77-101.
5. Gabriel JL, Milner R, Plaut GW. Inhibition and activation of bovine heart NAD-specific isocitrate dehydrogenase by ATP. *Arch Biochem Biophys*. 1985;240(1):128-134.
6. Frieden C. Glutamate Dehydrogenase. Vi. Survey of Purine Nucleotide and Other Effects on the Enzyme from Various Sources. *J Biol Chem*. 1965;240:2028-2035.
7. Hardie DG, Ross FA, Hawley SA. AMPK: a nutrient and energy sensor that maintains energy homeostasis. *Nat Rev Mol Cell Biol*. 2012;13(4):251-262.
8. Lin SC, Hardie DG. AMPK: Sensing Glucose as well as Cellular Energy Status. *Cell Metab*. 2018;27(2):299-313.
9. Hardie DG, Carling D. The AMP-activated protein kinase--fuel gauge of the mammalian cell? *Eur J Biochem*. 1997;246(2):259-273.
10. Pinho S, Frenette PS. Haematopoietic stem cell activity and interactions with the niche. *Nat Rev Mol Cell Biol*. 2019;20(5):303-320.
11. Crane GM, Jeffery E, Morrison SJ. Adult haematopoietic stem cell niches. *Nat Rev Immunol*. 2017;17(9):573-590.
12. de Haan G, Lazare SS. Aging of hematopoietic stem cells. *Blood*. 2018;131(5):479-487.
13. Mejia-Ramirez E, Florian MC. Understanding intrinsic hematopoietic stem cell aging. *Haematologica*. 2020;105(1):22-37.
14. Orkin SH, Zon LI. Hematopoiesis: an evolving paradigm for stem cell biology. *Cell*. 2008;132(4):631-644.
15. Nakada D, Saunders TL, Morrison SJ. Lkb1 regulates cell cycle and energy metabolism in haematopoietic stem cells. *Nature*. 2010;468(7324):653-658.
16. Gurumurthy S, Xie SZ, Alagesan B, et al. The Lkb1 metabolic sensor maintains haematopoietic stem cell

637 survival. *Nature*. 2010;468(7324):659-663.
638 17. Gan B, Hu J, Jiang S, et al. Lkb1 regulates quiescence and metabolic homeostasis of haematopoietic stem
639 cells. *Nature*. 2010;468(7324):701-704.
640 18. Sahin E, Colla S, Liesa M, et al. Telomere dysfunction induces metabolic and mitochondrial compromise.
641 *Nature*. 2011;470(7334):359-365.
642 19. Luchsinger LL, de Almeida MJ, Corrigan DJ, Mumau M, Snoeck HW. Mitofusin 2 maintains haematopoietic
643 stem cells with extensive lymphoid potential. *Nature*. 2016;529(7587):528-531.
644 20. de Almeida MJ, Luchsinger LL, Corrigan DJ, Williams LJ, Snoeck HW. Dye-Independent Methods Reveal
645 Elevated Mitochondrial Mass in Hematopoietic Stem Cells. *Cell Stem Cell*. 2017;21(6):725-729.e724.
646 21. Anso E, Weinberg SE, Diebold LP, et al. The mitochondrial respiratory chain is essential for haematopoietic
647 stem cell function. *Nat Cell Biol*. 2017;19(6):614-625.
648 22. Nakamura-Ishizu A, Matsumura T, Stumpf PS, et al. Thrombopoietin Metabolically Primes Hematopoietic
649 Stem Cells to Megakaryocyte-Lineage Differentiation. *Cell Rep*. 2018;25(7):1772-1785 e1776.
650 23. Qi L, Martin-Sandoval MS, Merchant S, et al. Aspartate availability limits hematopoietic stem cell function
651 during hematopoietic regeneration. *Cell Stem Cell*. 2021;28(11):1982-1999 e1988.
652 24. Filippi MD, Ghaffari S. Mitochondria in the maintenance of hematopoietic stem cells: new perspectives and
653 opportunities. *Blood*. 2019;133(18):1943-1952.
654 25. Guitart AV, Panagopoulou TI, Villacreces A, et al. Fumarate hydratase is a critical metabolic regulator of
655 hematopoietic stem cell functions. *J Exp Med*. 2017;214(3):719-735.
656 26. Hsu P, Qu CK. Metabolic plasticity and hematopoietic stem cell biology. *Curr Opin Hematol*. 2013;20(4):289-
657 294.
658 27. Busch K, Klapproth K, Barile M, et al. Fundamental properties of unperturbed haematopoiesis from stem cells
659 in vivo. *Nature*. 2015;518(7540):542-546.
660 28. Sun J, Ramos A, Chapman B, et al. Clonal dynamics of native haematopoiesis. *Nature*. 2014;514(7522):322-
661 327.
662 29. Ho TT, Warr MR, Adelman ER, et al. Autophagy maintains the metabolism and function of young and old
663 stem cells. *Nature*. 2017;543(7644):205-210.
664 30. Laurenti E, Gottgens B. From haematopoietic stem cells to complex differentiation landscapes. *Nature*.
665 2018;553(7689):418-426.
666 31. Nakamura-Ishizu A, Ito K, Suda T. Hematopoietic Stem Cell Metabolism during Development and Aging. *Dev*
667 *Cell*. 2020;54(2):239-255.
668 32. Takubo K, Nagamatsu G, Kobayashi CI, et al. Regulation of glycolysis by Pdk functions as a metabolic
669 checkpoint for cell cycle quiescence in hematopoietic stem cells. *Cell Stem Cell*. 2013;12(1):49-61.
670 33. Wang YH, Israelsen WJ, Lee D, et al. Cell-state-specific metabolic dependency in hematopoiesis and
671 leukemogenesis. *Cell*. 2014;158(6):1309-1323.
672 34. Simsek T, Kocabas F, Zheng J, et al. The distinct metabolic profile of hematopoietic stem cells reflects their
673 location in a hypoxic niche. *Cell Stem Cell*. 2010;7(3):380-390.

674 35. Inoue S, Noda S, Kashima K, Nakada K, Hayashi J, Miyoshi H. Mitochondrial respiration defects modulate
675 differentiation but not proliferation of hematopoietic stem and progenitor cells. *FEBS Lett*. 2010;584(15):3402-3409.
676 36. Yu WM, Liu X, Shen J, et al. Metabolic regulation by the mitochondrial phosphatase PTPMT1 is required for
677 hematopoietic stem cell differentiation. *Cell Stem Cell*. 2013;12(1):62-74.
678 37. Bejarano-Garcia JA, Millan-Ucles A, Rosado IV, et al. Sensitivity of hematopoietic stem cells to mitochondrial
679 dysfunction by SdhD gene deletion. *Cell Death Dis*. 2016;7(12):e2516.
680 38. Halvarsson C, Eliasson P, Jonsson JI. Pyruvate dehydrogenase kinase 1 is essential for transplantable mouse
681 bone marrow hematopoietic stem cell and progenitor function. *PLoS One*. 2017;12(2):e0171714.
682 39. Ito K, Carracedo A, Weiss D, et al. A PML–PPAR-δ pathway for fatty acid oxidation regulates hematopoietic
683 stem cell maintenance. *Nat Med*. 2012;18(9):1350-1358.
684 40. Karigane D, Kobayashi H, Morikawa T, et al. p38α Activates Purine Metabolism to Initiate Hematopoietic
685 Stem/Progenitor Cell Cycling in Response to Stress. *Cell Stem Cell*. 2016;19(2):192-204.
686 41. Umemoto T, Johansson A, Ahmad SAI, et al. ATP citrate lyase controls hematopoietic stem cell fate and
687 supports bone marrow regeneration. *EMBO J*. 2022:e109463.
688 42. Liang R, Arif T, Kalmykova S, et al. Restraining Lysosomal Activity Preserves Hematopoietic Stem Cell
689 Quiescence and Potency. *Cell Stem Cell*. 2020;26(3):359-376 e357.
690 43. Bowling S, Sritharan D, Osorio FG, et al. An Engineered CRISPR-Cas9 Mouse Line for Simultaneous
691 Readout of Lineage Histories and Gene Expression Profiles in Single Cells. *Cell*. 2020;181(6):1410-1422 e1427.
692 44. Fanti AK, Busch K, Greco A, et al. Flt3- and Tie2-Cre tracing identifies regeneration in sepsis from
693 multipotent progenitors but not hematopoietic stem cells. *Cell Stem Cell*. 2023;30(2):207-218 e207.
694 45. Munz CM, Dressel N, Chen M, Grinenko T, Roers A, Gerbaulet A. Regeneration following blood loss and
695 acute inflammation proceeds without contribution of primitive HSCs. *Blood*. 2023.
696 46. Agathocleous M, Meacham CE, Burgess RJ, et al. Ascorbate regulates haematopoietic stem cell function and
697 leukaemogenesis. *Nature*. 2017;549(7673):476-481.
698 47. DeVilbiss AW, Zhao Z, Martin-Sandoval MS, et al. Metabolomic profiling of rare cell populations isolated by
699 flow cytometry from tissues. *Elife*. 2021;10.
700 48. Lengefeld J, Cheng CW, Maretich P, et al. Cell size is a determinant of stem cell potential during aging. *Sci*
701 *Adv*. 2021;7(46):eabk0271.
702 49. Schonberger K, Obier N, Romero-Mulero MC, et al. Multilayer omics analysis reveals a non-classical retinoic
703 acid signaling axis that regulates hematopoietic stem cell identity. *Cell Stem Cell*. 2022;29(1):131-148 e110.
704 50. Jun S, Mahesula S, Mathews TP, et al. The requirement for pyruvate dehydrogenase in leukemogenesis
705 depends on cell lineage. *Cell Metab*. 2021;33(9):1777-1792 e1778.
706 51. Imamura H, Nhat KP, Togawa H, et al. Visualization of ATP levels inside single living cells with fluorescence
707 resonance energy transfer-based genetically encoded indicators. *Proc Natl Acad Sci U S A*. 2009;106(37):15651-15656.
708 52. Nakano M, Imamura H, Nagai T, Noji H. Ca(2)(+) regulation of mitochondrial ATP synthesis visualized at the
709 single cell level. *ACS Chem Biol*. 2011;6(7):709-715.
710 53. Yamamoto M, Kim M, Imai H, Itakura Y, Ohtsuki G. Microglia-Triggered Plasticity of Intrinsic Excitability

711 Modulates Psychomotor Behaviors in Acute Cerebellar Inflammation. *Cell Rep*. 2019;28(11):2923-2938 e2928.
712 54. Oki T, Nishimura K, Kitaura J, et al. A novel cell-cycle-indicator, mVenus-p27K-, identifies quiescent cells and
713 visualizes G0-G1 transition. *Sci Rep*. 2014;4:4012.
714 55. Fukushima T, Tanaka Y, Hamey FK, et al. Discrimination of Dormant and Active Hematopoietic Stem Cells by
715 G0 Marker Reveals Dormancy Regulation by Cytoplasmic Calcium. *Cell Rep*. 2019;29(12):4144-4158 e4147.
716 56. Miyajima M, Zhang B, Sugiura Y, et al. Metabolic shift induced by systemic activation of T cells in PD-1-
717 deficient mice perturbs brain monoamines and emotional behavior. *Nat Immunol*. 2017;18(12):1342-1352.
718 57. Arai F, Hirao A, Ohmura M, et al. Tie2/angiopoietin-1 signaling regulates hematopoietic stem cell quiescence
719 in the bone marrow niche. *Cell*. 2004;118(2):149-161.
720 58. Miller I, Min M, Yang C, et al. Ki67 is a Graded Rather than a Binary Marker of Proliferation versus
721 Quiescence. *Cell Rep*. 2018;24(5):1105-1112 e1105.
722 59. Dunaway GA. A review of animal phosphofructokinase isozymes with an emphasis on their physiological role.
723 *Mol Cell Biochem*. 1983;52(1):75-91.
724 60. Yalcin A, Telang S, Clem B, Chesney J. Regulation of glucose metabolism by 6-phosphofructo-2-
725 kinase/fructose-2,6-bisphosphatases in cancer. *Exp Mol Pathol*. 2009;86(3):174-179.
726 61. Marsin AS, Bouzin C, Bertrand L, Hue L. The stimulation of glycolysis by hypoxia in activated monocytes is
727 mediated by AMP-activated protein kinase and inducible 6-phosphofructo-2-kinase. *J Biol Chem*. 2002;277(34):30778-
728 30783.
729 62. Hardie DG. AMPK--sensing energy while talking to other signaling pathways. *Cell Metab*. 2014;20(6):939-
730 952.
731 63. Long YC, Zierath JR. AMP-activated protein kinase signaling in metabolic regulation. *J Clin Invest*.
732 2006;116(7):1776-1783.
733 64. Shi L, Pan H, Liu Z, Xie J, Han W. Roles of PFKFB3 in cancer. *Signal Transduct Target Ther*. 2017;2:17044.
734 65. Novellasdemunt L, Bultot L, Manzano A, et al. PFKFB3 activation in cancer cells by the p38/MK2 pathway in
735 response to stress stimuli. *Biochem J*. 2013;452(3):531-543.
736 66. Okamura N, Sakakibara R. A common phosphorylation site for cyclic AMP-dependent protein kinase and
737 protein kinase C in human placental 6-phosphofructo-2-kinase/fructose-2,6-bisphosphatase. *Biosci Biotechnol Biochem*.
738 1998;62(10):2039-2042.
739 67. Yamamoto T, Takano N, Ishiwata K, et al. Reduced methylation of PFKFB3 in cancer cells shunts glucose
740 towards the pentose phosphate pathway. *Nat Commun*. 2014;5:3480.
741 68. Kobayashi H, Morikawa T, Okinaga A, et al. Environmental Optimization Enables Maintenance of Quiescent
742 Hematopoietic Stem Cells Ex Vivo. *Cell Rep*. 2019;28(1):145-158 e149.
743 69. Shiroshita K, Kobayashi H, Watanuki S, et al. A culture platform to study quiescent hematopoietic stem cells
744 following genome editing. *Cell Rep Methods*. 2022;2(12):100354.
745 70. Intlekofer AM, Finley LWS. Metabolic signatures of cancer cells and stem cells. *Nat Metab*. 2019;1(2):177-
746 188.
747 71. Takubo K, Goda N, Yamada W, et al. Regulation of the HIF-1alpha level is essential for hematopoietic stem

748 cells. *Cell Stem Cell*. 2010;7(3):391-402.
749 72. Signer RA, Magee JA, Salic A, Morrison SJ. Haematopoietic stem cells require a highly regulated protein
750 synthesis rate. *Nature*. 2014;509(7498):49-54.
751 73. Essers MA, Offner S, Blanco-Bose WE, et al. IFNalpha activates dormant haematopoietic stem cells in vivo.
752 *Nature*. 2009;458(7240):904-908.
753 74. Umemoto T, Hashimoto M, Matsumura T, Nakamura-Ishizu A, Suda T. Ca(2+)-mitochondria axis drives cell
754 division in hematopoietic stem cells. *J Exp Med*. 2018;215(8):2097-2113.
755 75. Maryanovich M, Zaltsman Y, Ruggiero A, et al. An MTCH2 pathway repressing mitochondria metabolism
756 regulates haematopoietic stem cell fate. *Nat Commun*. 2015;6:7901.
757 76. Ito K, Carracedo A, Weiss D, et al. A PML-PPAR-delta pathway for fatty acid oxidation regulates
758 hematopoietic stem cell maintenance. *Nat Med*. 2012;18(9):1350-1358.
759 77. Webb BA, Forouhar F, Szu FE, Seetharaman J, Tong L, Barber DL. Structures of human phosphofructokinase-
760 1 and atomic basis of cancer-associated mutations. *Nature*. 2015;523(7558):111-114.
761 78. Zhu L, He X, Dong H, et al. Protein arginine methyltransferase 1 is required for maintenance of normal adult
762 hematopoiesis. *Int J Biol Sci*. 2019;15(13):2763-2773.
763

764 **Figure Legends**

765 **Figure 1. HSC cell cycling increases overall glycolytic flux, but not flux into mitochondria.**

766 **(A)** Experimental design used for glucose isotope tracer analysis in HSCs from 5-FU- or PBS-treated
767 mice. **(B)** Heat map of metabolite levels in HSCs derived from mice treated with PBS or 5-FU. **(C-F)**
768 Relative amounts of U-$^{13}C_6$-glucose-derived metabolites in glycolysis (C), the first round of TCA
769 cycle (D), the PPP €, and nucleotide synthesis (F) in HSCs from 5-FU- or PBS-treated mice (PBS
770 group = 1.0); In (B)-(F), biological replicates from the PBS and 5-FU groups, obtained on three
771 separate days, were pooled, analyzed by IC-MS, quantified based on calibration curve data for each
772 metabolite (see "**Ion chromatography mass spectrometry (IC-MS) analysis**" section in
773 "**Methods**" for details). **(G)** Experimental schema of *in vivo* 2-NBDG analysis. **(H)** Representative
774 histograms of 2-NBDG analysis (gray: no 2-NBDG, red: PBS group, blue: 5-FU group). **(I)** 2-NBDG
775 positivity in each fraction; data represent four pooled biological replicates for the PBS group and
776 three for the 5-FU group; MyP: myeloid progenitor. **(J)** EPCR expression and 2-NBDG positivity
777 within HSC fractions. Data were extracted from each individual in (I).

778 Data are presented as mean ± SD. * $p \leq 0.05$, ** $p \leq 0.01$, *** $p \leq 0.001$ as determined by paired-
779 samples *t*-test (C-F) and Student's *t*-test (I and J). Abbreviations: G6P, glucose-6-phosphate; F6P,
780 fructose-6-phosphate; F1,6BP, fructose-1,6-bisphosphate; G3P, glycerol-3-phosphate; DHAP,
781 dihydroxyacetone phosphate; 3PG, 3-phosphoglycerate; 2PG, 2-phosphoglycerate; PEP,
782 phosphoenolpyruvate; PYR, pyruvate; LAC, lactate; Ac-CoA; acetyl-CoA; CIT, citrate; ACO, cis-
783 aconitic acid, isocitrate; 2OG, 2-oxoglutarate; SUC, succinate; FUM, fumarate; MAL, malate; OAA,
784 oxaloacetate; 6PG, glucose-6-phosphate; Ru5P, ribulose-5-phosphate; Xu5P, xylulose-5-phosphate;
785 R5P, ribose-5-phosphate; S7P, sedoheptulose-7-phosphate; E4P, erythrose-4-phosphate; PRPP,
786 phosphoribosyl pyrophosphate; IMP, inosine monophosphate; ATP, adenosine triphosphate; GTP,
787 guanine triphosphate; UMP, uridine monophosphate; UTP, uridine triphosphate; TTP, thymidine
788 triphosphate. See also Fig. S1 and S2.

789

790 **Figure 2. OXPHOS inhibition activates compensatory glycolysis in HSCs.**

791 **(A)** Experimental design used for glucose isotope tracer analysis in HSCs treated with the OXPHOS
792 inhibitor oligomycin. **(B)** Heat map of metabolite levels detected by *in vitro* tracer analysis of U-
793 $^{13}C_6$-glucose in HSCs treated with DMSO or oligomycin (Oligo). **(C-F)** Relative amounts of U-$^{13}C_6$-
794 glucose-derived metabolites in glycolysis (C), the first round of TCA cycle (D), the P€(E), and
795 nucleotide synthesis (F) in DMSO- (black) or oligomycin-treated (orange) HSCs; In (B)-(F),

796 biological replicates of the DMSO and oligomycin groups obtained on four separate days were
797 pooled, analyzed by IC-MS, and quantified based on calibration curve data for each metabolite (see
798 "**Ion chromatography mass spectrometry (IC-MS) analysis**" section in "**Methods**" for details).
799 (G-H) Overview of the Mito Stress test on the Seahorse flux analyzer for HSC and MyPs; (G) ECAR
800 before and after oligomycin treatment (H). (Data were obtained from n = 3 technical replicates for
801 HSCs and n = 10 technical replicates for MyPs.)
802 Data are shown as mean ± SD. * $p \leq 0.05$, ** $p \leq 0.01$, *** $p \leq 0.001$ as determined by paired-
803 samples t-test (C-E) and Student's *t*-test (H). Abbreviations: G6P, glucose-6-phosphate; F6P,
804 fructose-6-phosphate; F1,6BP, fructose-1,6-bisphosphate; G3P, glycerol-3-phosphate; DHAP,
805 dihydroxyacetone phosphate; 3PG, 3-phosphoglycerate; 2PG, 2-phosphoglycerate; PEP,
806 phosphoenolpyruvate; PYR, pyruvate; LAC, lactate; Ac-CoA; acetyl-CoA; CIT, citrate; ACO, cis-
807 aconitic acid, isocitrate; 2OG, 2-oxoglutarate; SUC, succinate; FUM, fumarate; MAL, malate; OAA,
808 oxaloacetate; 6PG, glucose-6-phosphate; Ru5P, ribulose-5-phosphate; Xu5P, xylulose-5-phosphate;
809 R5P, ribose-5-phosphate; S7P, sedoheptulose-7-phosphate; E4P, erythrose-4-phosphate; PRPP,
810 phosphoribosyl pyrophosphate; IMP, inosine monophosphate; ATP, adenosine triphosphate; GTP,
811 guanine triphosphate; UMP, uridine monophosphate; UTP, uridine triphosphate; TTP, thymidine
812 triphosphate. See also Fig. S2.
813
814 **Figure 3. Quantitative ^{13}C-MFA of quiescent, proliferative, and stressed HSCs**
815 **(A-C)** Overview of quantitative ^{13}C-MFA of PBS-treated HSCs (A), 5-FU-treated HSCs (B), and
816 OXPHOS-inhibited HSCs (C). The representative net flux for each reaction with glucose uptake as
817 100 is shown in the squares below the catalytic enzymes for each reaction listed in green letters. Red
818 arrows indicate reactions with particularly elevated fluxes and blue arrows indicate reactions with
819 particularly decreased fluxes. (D) Heatmap of the relative flux of each enzyme in the 5-FU or
820 oligomycin groups compared to that in the quiescent (Ctl) HSC (The metabolic flux of each enzyme
821 in the Ctl group was standardized as 100.). **(E-J)** Fluxes due to reactions with PFK (E, H), G6PD (F,
822 I), and PDH (G, J). Fluxes of HSCs derived from mice treated with 5-FU (blue bars) or PBS (red
823 bars) (D-F) and of HSCs treated with DMSO (black bars) or oligomycin (orange bars) (G-I) are
824 shown. Data is obtained from 100 simulations in OpenMebius, and flux data for each enzyme is
825 displayed (Table S4). **(K-L)** Ratio of fructose 1,6-bisphosphate (F1,6BP) to fructose-6-phosphate
826 (F6P) calculated from tracer experiments shown in Figure 1B and Figure 2B. Effects of 5-FU
827 administration (K) or mitochondrial inhibition by oligomycin (L) are summarized. Data are shown as

828 mean ± SD. * $p \leq 0.05$, ** $p \leq 0.01$, *** $p \leq 0.001$ as determined by Student's *t*-test (E-L).
829 Abbreviations: HK, hexokinase; PGI, glucose-6-phosphate isomerase; PFK, phosphofructokinase;
830 TPI, triose phosphate isomerase; GAPDH, glyceraldehyde-3-phosphate dehydrogenase; PGM,
831 phosphoglycerate mutase; PK, pyruvate kinase; LDH, lactate dehydrogenase; PC, pyruvate
832 carboxylase; PDH, pyruvate dehydrogenase; CS; citrate synthase; IDH, isocitrate dehydrogenase;
833 αKGDH, α-ketoglutaric acid dehydrogenase; SDH, succinate dehydrogenase; G6PD, glucose-6-
834 phosphate dehydrogenase; TAL, transaldolase. See also Fig. S3.
835
836 **Figure 4. Pfkfb3 activates the glycolytic system in proliferating HSCs**
837 **(A)** Experimental design used to conduct real-time ATP analysis of HSCs treated with 5-FU or PBS.
838 PLFA medium containing mitochondrial substrates (pyruvate, lactate, fatty acids, and amino acids)
839 but no glucose, was used for experiments with 2-DG; Ba-M containing neither mitochondrial
840 substrates nor glucose was used for experiments with oligomycin, Pfkfb3 inhibitor, or AMPK
841 inhibitor. **(B-I)** Results of real-time ATP analysis of PBS- (red) or 5-FU-treated (blue) HSCs after
842 treatment with 2-DG (B, D), oligomycin (C, E), PFKFB3 inhibitor (F, H), or AMPK inhibitor (G, I).
843 Bar graphs show corrected ATP concentrations for the last 2 min (D) of (B), 6–7 min (E) of (C), or
844 the last 1 min (H, I) of (F, G) for PFKFB3 and AMPK inhibitors, respectively. Each group represents
845 at least 60 cells. Data are representative results of pooled samples from three biological replicates.
846 (see "**Time-course analysis of FRET values**" in "**Supplementary Methods**" for details of the
847 correction method used to calculate ATP concentration.)
848 Data are presented as mean ± SD. * $p \leq 0.05$, ** $p \leq 0.01$, *** $p \leq 0.001$ as determined by Student's
849 *t*-test (D, E, H, and I). See also Fig. S5.
850
851 **Figure 5. PFKFB3 accelerates glycolysis in HSCs under OXPHOS inhibition in an AMPK-**
852 **dependent manner**
853 **(A)** Experimental design of real-time ATP analysis using GO-ATeam2 knock-in BMMNCs. Ba-M
854 was used in experiments with oligomycin. For other experiments, PLFA medium was used. **(B-C)**
855 Evaluation of factors affecting ATP concentration in HSCs (B) and GMPs (C) based on the GO-
856 ATeam2 system. GO-ATeam2 knock-in BMMNCs were incubated with glucose, oligomycin, 2-DG,
857 or glucose plus oligomycin, and the FRET/EGFP ratio was calculated. **(D)** ATP concentration in
858 indicated stem/progenitor fractions in PLFA medium (red bars) alone or PLFA medium plus 2-DG
859 (blue bars). ATP concentration for the last 2 min of the analysis time is shown. Data is summarized

860 from Figure 5B-C and Supplemental Figure 5A-D. Each group represents at least 110 cells. Data are
861 representative results of pooled samples from three biological replicates. **(E)** ATP concentration in
862 indicated stem/progenitor fractions in Ba-M plus glucose (dark blue bars) or Ba-M plus glucose and
863 oligomycin (orange bars). ATP concentration for the last 1 min of the analysis period is shown. Data
864 is summarized from Figure 5B-C and Supplemental Figure 5A-D. Each group represents at least 43
865 cells. Data are representative results of pooled samples from three biological replicates. **(F-I)** Effects
866 of PFKFB3 or AMPK inhibitors (PFKFB3i or AMPKi, respectively) on ATP concentration in HSCs
867 from GO-ATeam2 mice in Ba-M plus glucose only (F) or Ba-M plus glucose and oligomycin (G).
868 ATP concentrations for the last 1 min of the analysis period are shown in (H) and (I) for glucose only
869 and glucose with oligomycin groups, respectively. Each group represents at least 90 cells. Data are
870 representative results of pooled samples from three biological replicates. **(J)** Experimental schema
871 for cell cycle assay and real-time ATP concentration analysis after overexpression of *Pfkfb3*. **(K)** Cell
872 cycle status of *Pfkfb3*-overexpressing (*Pfkfb3*OE) and *mock*-transduced HSCs. **(L-O)** Effects of
873 inhibitors on ATP concentration in *Pfkfb3*-overexpressing GO-ATeam2^{+} HSCs. Cells were exposed to
874 vehicle (Ctl) (L), 2-DG (M), oligomycin (N), or glucose 12.5 mg/dL and oligomycin (O), and ATP
875 concentrations for the last 1 (L, N, and O) or 2 min (M) of the analysis period were calculated. Data
876 are representative results of pooled samples from three biological replicates.
877 Data are presented as mean ± SD. * $p \leq 0.05$, ** $p \leq 0.01$, *** $p \leq 0.001$ as determined by Student's
878 *t*-test (D, E, and K-O) or one-way ANOVA followed by Tukey's test (H and I). See also Fig. S5.
879

880 **Figure 6. PFKFB3 methylation by PRMT1 enables ATP production by cell-cycling HSCs.**
881 **(A)** Normalized *Pfkfb3* mRNA counts based on RNA sequencing of PBS-treated (red) or 5-FU-
882 treated (blue) HSCs. Data are representative results of pooled samples from three biological
883 replicates. **(B)** Quantification of mean fluorescent intensity (MFI) of PFKFB3 protein in PBS- or 5-
884 FU-treated HSCs. The lower part of the graph shows representative images of
885 immunocytochemistry of PFKFB3 in each group. n = 26–27 single HSCs for each group. The data
886 are representative results from two independent experiments. **(C)** Quantification of MFI of
887 phosphorylated-PFKFB3 (p-PFKFB3) protein in PBS- or 5-FU-treated HSCs. The lower part of the
888 graph shows representative images of immunocytochemistry of p-PFKFB3 in each group. n = 27
889 single HSCs for each group. The data are representative results from two independent experiments.
890 **(D)** Quantification of mean fluorescence intensity (MFI) of p-PFKFB3 in HSCs treated with glucose
891 (200mg/dL); glucose plus oligomycin (1 μM); and glucose, oligomycin, and dorsomorphin (100 μM)

892 for 5 min. The lower part of the graph shows representative images of immunocytochemistry of p-
893 PFKFB3 in each group. n = 32–36 for each group. The data are representative results from two
894 independent experiments. **(E)** Normalized *Prmt1* mRNA counts based on RNA sequencing of PBS-
895 treated (red) or 5-FU-treated (blue) HSCs. Data are representative results of pooled samples from
896 three biological replicates. **(F)** MFI quantification of methylated-PFKFB3 (m-PFKFB3) in PBS- or
897 5-FU-treated HSCs. The lower part of the graph shows representative images of
898 immunocytochemistry of m-PFKFB3 in each group. n = 23–41 for each group. The data are
899 representative results from three independent experiments. **(G)** Quantification of MFI of m-PFKFB3
900 in PBS- or 5-FU-treated HSCs or 5-FU-treated HSCs after 15 min treatment with a PRMT1 inhibitor
901 (90 μg/mL GSK3368715); n = 25–35 single HSCs for each group. The lower part of the graph shows
902 representative images showing immunocytochemistry of m-PFKFB3. Data represent a single
903 experiment. **(H)** Quantitation of m-PFKFB3 in NBDG-positive or -negative HSCs in mice treated
904 with PBS or 5-FU. The lower part of the graph shows representative images of
905 immunocytochemistry of m-PFKFB3 in each group. n = 28–41 for each group. The data are
906 representative results from two independent experiments. **(I-J)** Corrected ATP levels in PBS- (red) or
907 5-FU-treated (blue) HSCs 15 min after treatment with vehicle (I) or a PRMT1 inhibitor (90 μg/mL
908 GSK3368715) (J). Each group represents at least 101 cells. Data are representative results of pooled
909 samples of two biological replicates. (see "**Time-course analysis of FRET values**" in
910 "**Supplementary Methods**" for details of the correction method used to calculate ATP
911 concentration.) Data are presented as mean ± SD. * $p \leq 0.05$, ** $p \leq 0.01$, *** $p \leq 0.001$ as
912 determined by Student's *t*-test (A-C, E-F, and I-J) or one-way ANOVA followed by Tukey's test (D,
913 G, and H).
914
915 **Figure 7. PFKFB3 maintains HSC function under proliferative stress.**
916 **(A-C)** Transplant analysis of *Pfkfb3*-KO or *Pfkfb3*CA-overexpressing HSCs. Experimental design
917 (A). PB chimerism of donor-derived cells at 4 months post-transplant. *Pfkfb3*-KO group, n = 6;
918 *Rosa*-KO group, n = 4; (B) *Pfkfb3* group, n = 5; pMY-IRES-GFP group, n = 4. (C) The data are
919 representative results from two independent experiments. **(D-E)** 5-FU administration after bone
920 marrow reconstruction with *Pfkfb3*- or *Rosa*-KO HSPCs. Experimental schema (D). Behavior of the
921 *Pfkfb3*- or *Rosa*-KO cells in PB after 5-FU administration (E). n = 5 for each group. **(F-K)** Cell cycle
922 analysis and apoptosis assay of *Pfkfb3*- or *Rosa*-KO HSPCs on day 2 post-BMT. Experimental
923 schema (F). Representative plots of Ki67/Hoechst33432 staining of *Rosa*-KO (G) or *Pfkfb3*-KO (H)

924 HSPCs and summary of analysis (I); summary of *in vivo* BrdU labeling assay (J). Apoptosis assay
925 results (K). n = 4–5 biological replicates for each group. **(L-N)** Cell cycle analysis of *Pfkfb3*CA or
926 *Mock*-overexpressing HSPCs on day 2 after BMT. Experimental Schema (L). Representative plot of
927 Ki67/Hoechst33432 staining for both groups (M) and summary of analysis (N). n = 5 biological
928 replicates for each group. **(O)** Models showing ATP production and regulation in quiescent,
929 OXPHOS-inhibited, and cell-cycling HSCs. Note that the GO-ATeam2 system identified plastic
930 acceleration of glycolysis by PFKFB3 in response to different types of stress maintains ATP levels.
931 Data are presented as mean ± SD. * $p \leq 0.05$, ** $p \leq 0.01$, *** $p \leq 0.001$ as determined by Student's
932 *t*-test (B, C, E, H, J, K, and N).
933

Figure 1

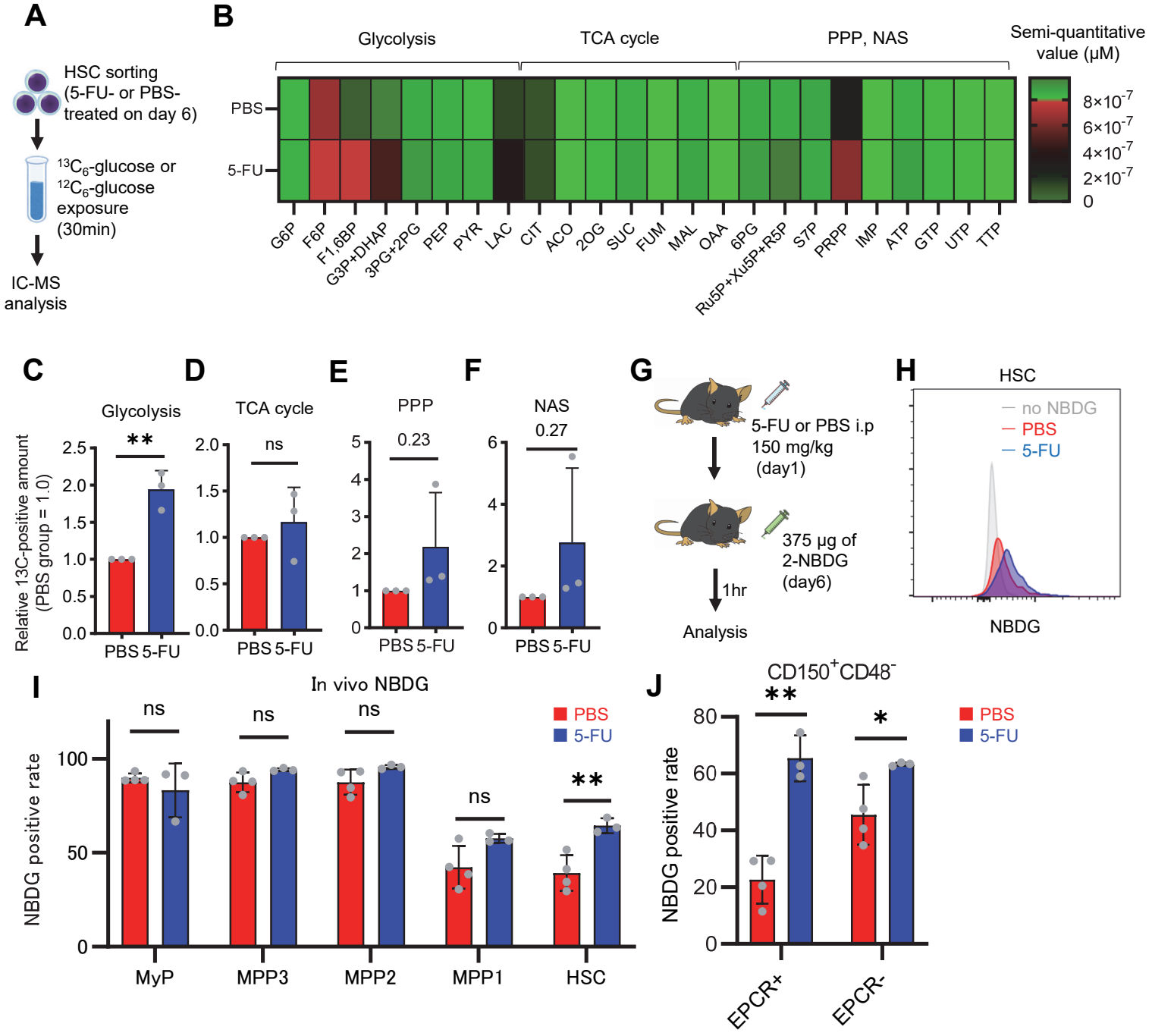
A
HSC sorting (5-FU- or PBS-treated on day 6)
$^{13}C_6$-glucose or $^{12}C_6$-glucose exposure (30min)
IC-MS analysis
B
Glycolysis
TCA cycle
PPP, NAS
Semi-quantitative value (μM)
PBS
5-FU
G6P F6P F1,6BP G3P+DHAP 3PG+2PG PEP PYR LAC CIT ACO 2OG SUC FUM MAL OAA 6PG Ru5P+Xu5P+R5P S7P PRPP IMP ATP GTP UTP TTP
8×10-7
6×10-7
4×10-7
2×10-7
0
C
Glycolysis
Relative 13C-positive amount (PBS group = 1.0)
**
PBS 5-FU
D
TCA cycle
ns
PBS 5-FU
E
PPP
0.23
PBS 5-FU
F
NAS
0.27
PBS 5-FU
G
5-FU or PBS i.p 150 mg/kg (day1)
375 μg of 2-NBDG (day6)
1hr
Analysis
H
HSC
no NBDG
PBS
5-FU
NBDG
I
In vivo NBDG
NBDG positive rate
ns
ns
ns
ns
**
PBS
5-FU
MyP
MPP3
MPP2
MPP1
HSC
J
CD150+CD48-
NBDG positive rate
**
*
PBS
5-FU
EPCR+
EPCR-

Figure 2

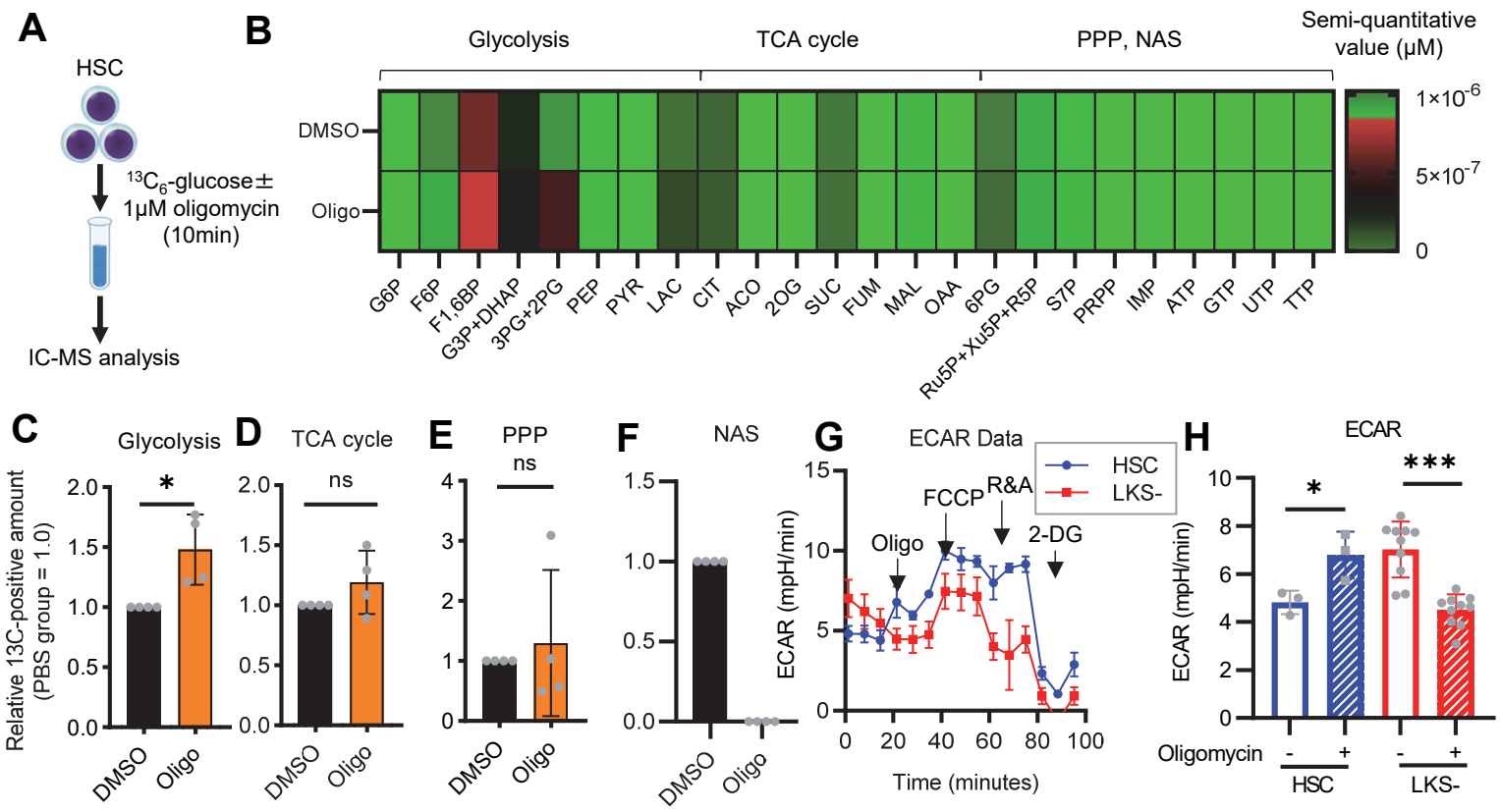
A
HSC
$^{13}C_6$-glucose±
1μM oligomycin
(10min)
IC-MS analysis
B
Glycolysis
TCA cycle
PPP, NAS
Semi-quantitative value (μM)
DMSO
Oligo
1×10-6
5×10-7
0
G6P
F6P
F1,6BP
G3P+DHAP
3PG+2PG
PEP
PYR
LAC
CIT
ACO
2OG
SUC
FUM
MAL
OAA
6PG
Ru5P+Xu5P+R5P
S7P
PRPP
IMP
ATP
GTP
UTP
TTP
C
Glycolysis
Relative 13C-positive amount (PBS group = 1.0)
*
DMSO
Oligo
D
TCA cycle
ns
E
PPP
ns
F
NAS
G
ECAR Data
HSC
LKS-
Oligo
FCCP
R&A
2-DG
ECAR (mpH/min)
Time (minutes)
H
ECAR
*
***
Oligomycin
HSC
LKS-

Figure 3

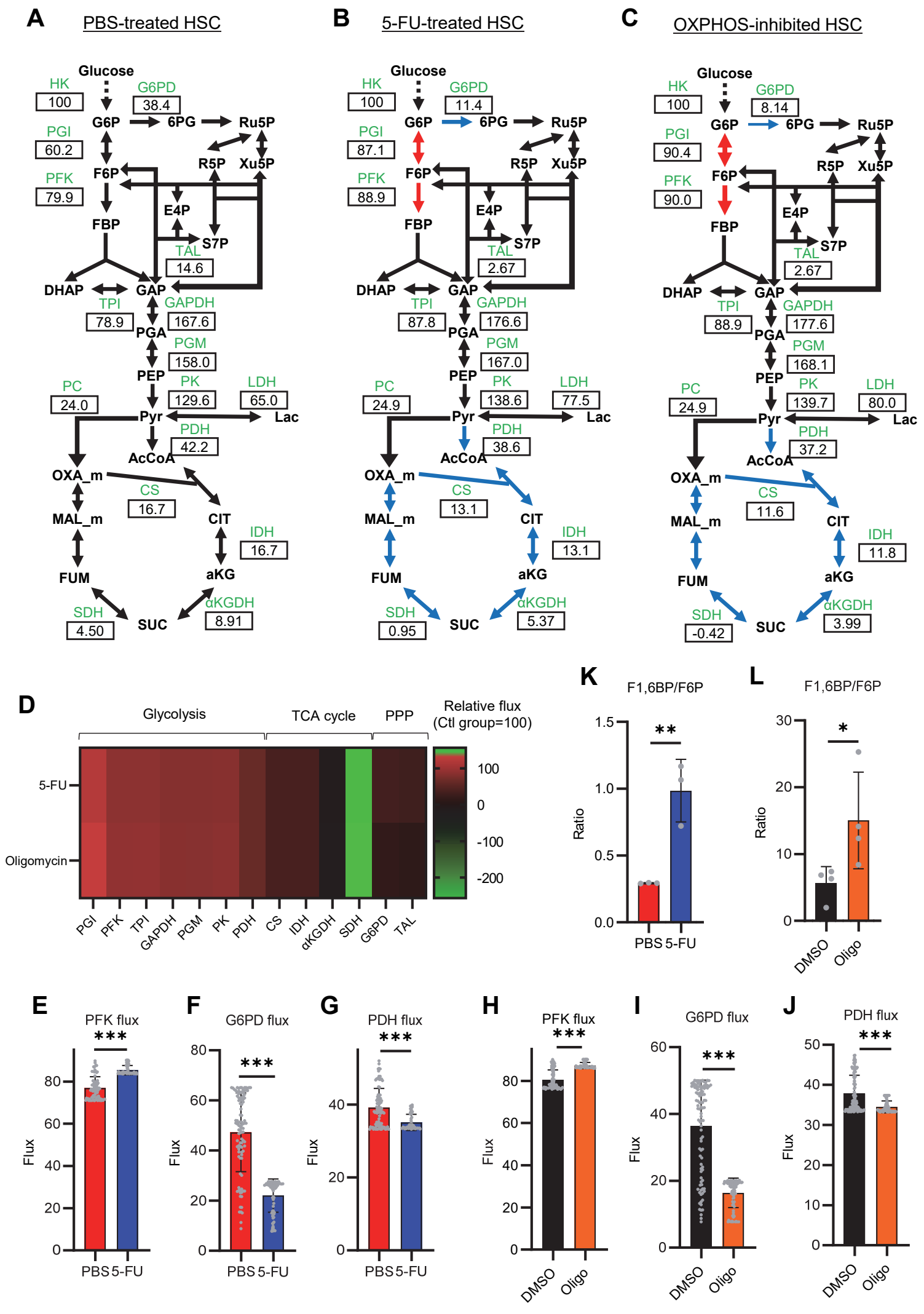
A
PBS-treated HSC
B
5-FU-treated HSC
C
OXPHOS-inhibited HSC
Glucose
HK
G6PD
PGI
PFK
TAL
TPI
GAPDH
PGM
PK
LDH
PC
PDH
CS
IDH
αKGDH
SDH
G6P
6PG
Ru5P
R5P
Xu5P
F6P
E4P
FBP
S7P
DHAP
GAP
PGA
PEP
Pyr
Lac
AcCoA
OXA_m
MAL_m
CIT
FUM
aKG
SUC
D
Glycolysis
TCA cycle
PPP
Relative flux
(Ctl group=100)
5-FU
Oligomycin
PGI
PFK
TPI
GAPDH
PGM
PK
PDH
CS
IDH
αKGDH
SDH
G6PD
TAL
K
F1,6BP/F6P
Ratio
PBS
5-FU
L
F1,6BP/F6P
DMSO
Oligo
E
PFK flux
F
G6PD flux
G
PDH flux
H
PFK flux
I
G6PD flux
J
PDH flux
Flux

Figure 4

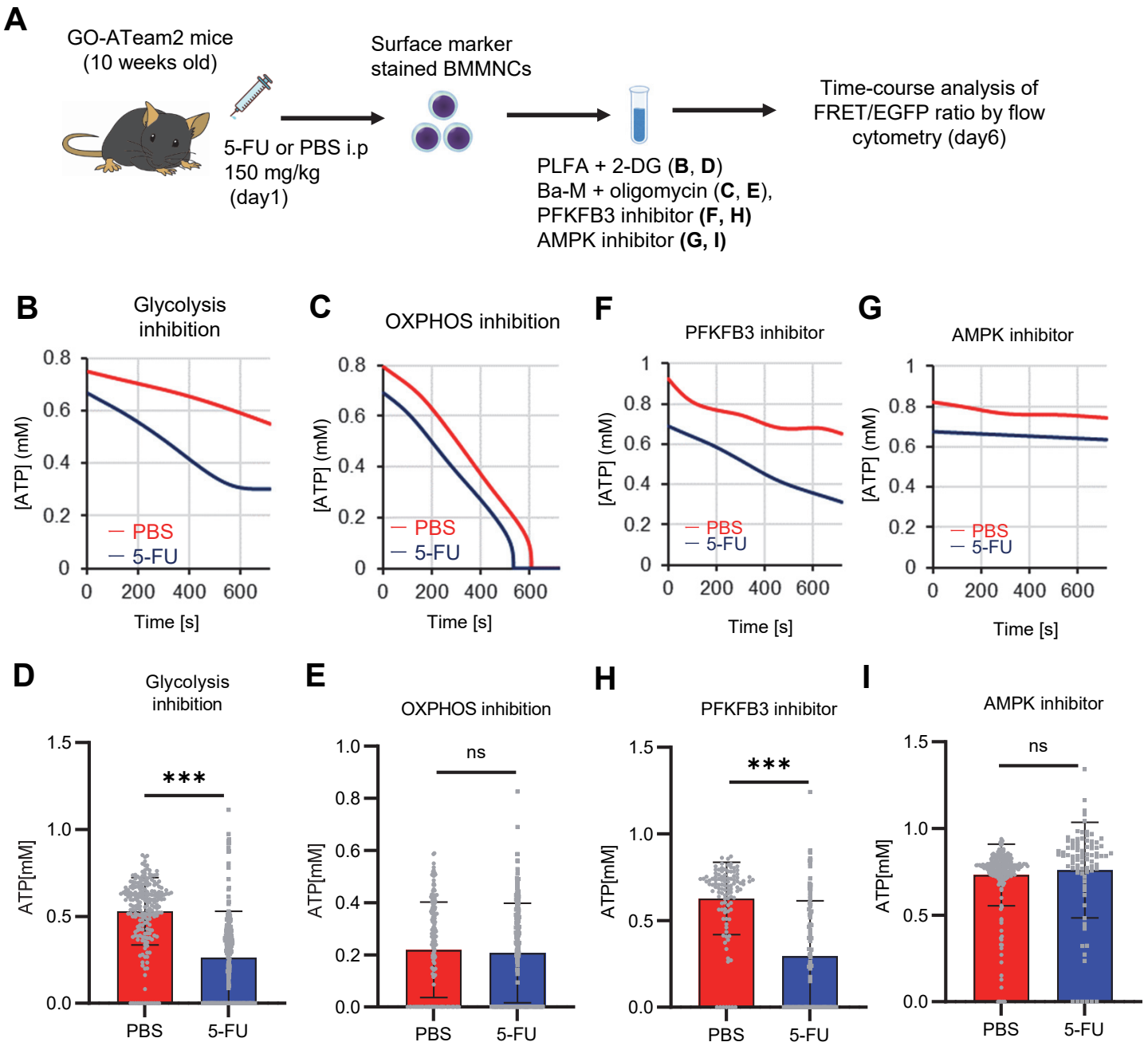
A
GO-ATeam2 mice
(10 weeks old)
5-FU or PBS i.p
150 mg/kg
(day1)
Surface marker
stained BMMNCs
PLFA + 2-DG (B, D)
Ba-M + oligomycin (C, E),
PFKFB3 inhibitor (F, H)
AMPK inhibitor (G, I)
Time-course analysis of
FRET/EGFP ratio by flow
cytometry (day6)
B
Glycolysis
inhibition
C
OXPHOS inhibition
F
PFKFB3 inhibitor
G
AMPK inhibitor
[ATP] (mM)
Time [s]
PBS
5-FU
D
Glycolysis
inhibition
E
OXPHOS inhibition
H
PFKFB3 inhibitor
I
AMPK inhibitor
ATP[mM]
***
ns
PBS
5-FU

Figure 5

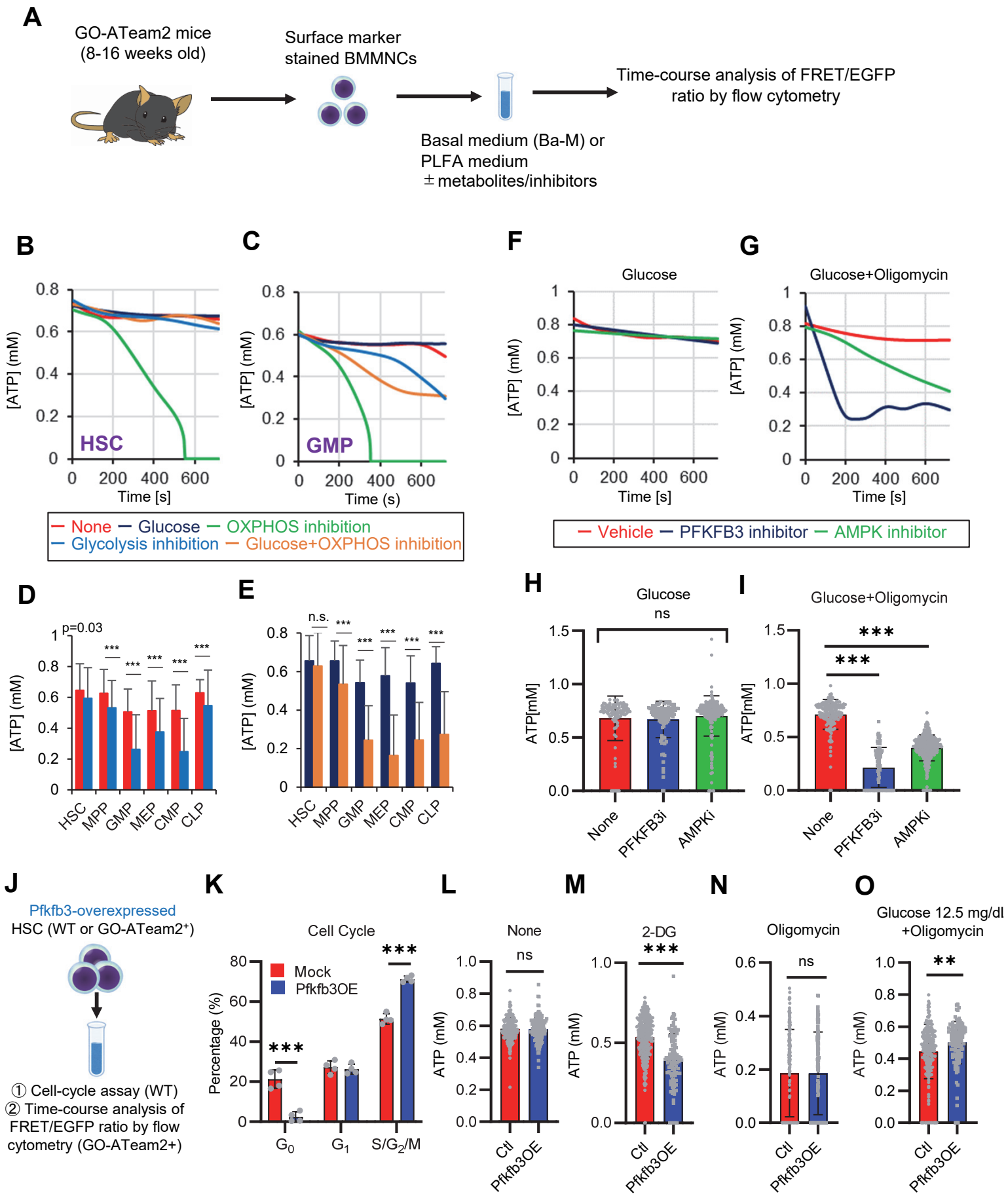
A
GO-ATeam2 mice
(8-16 weeks old)
Surface marker
stained BMMNCs
Basal medium (Ba-M) or
PLFA medium
± metabolites/inhibitors
Time-course analysis of FRET/EGFP
ratio by flow cytometry
B
C
HSC
GMP
[ATP] (mM)
Time [s]
Time (s)
None
Glucose
OXPHOS inhibition
Glycolysis inhibition
Glucose+OXPHOS inhibition
F
G
Glucose
Glucose+Oligomycin
Vehicle
PFKFB3 inhibitor
AMPK inhibitor
D
E
p=0.03
n.s.
HSC
MPP
GMP
MEP
CMP
CLP
H
I
ATP[mM]
None
PFKFB3i
AMPKi
J
Pfkfb3-overexpressed
HSC (WT or GO-ATeam2+)
① Cell-cycle assay (WT)
② Time-course analysis of
FRET/EGFP ratio by flow
cytometry (GO-ATeam2+)
K
Cell Cycle
Mock
Pfkfb3OE
Percentage (%)
G0
G1
S/G2/M
L
None
ns
M
2-DG
N
Oligomycin
O
Glucose 12.5 mg/dl
+Oligomycin
ATP (mM)
Ctl
Pfkfb3OE

Figure 6

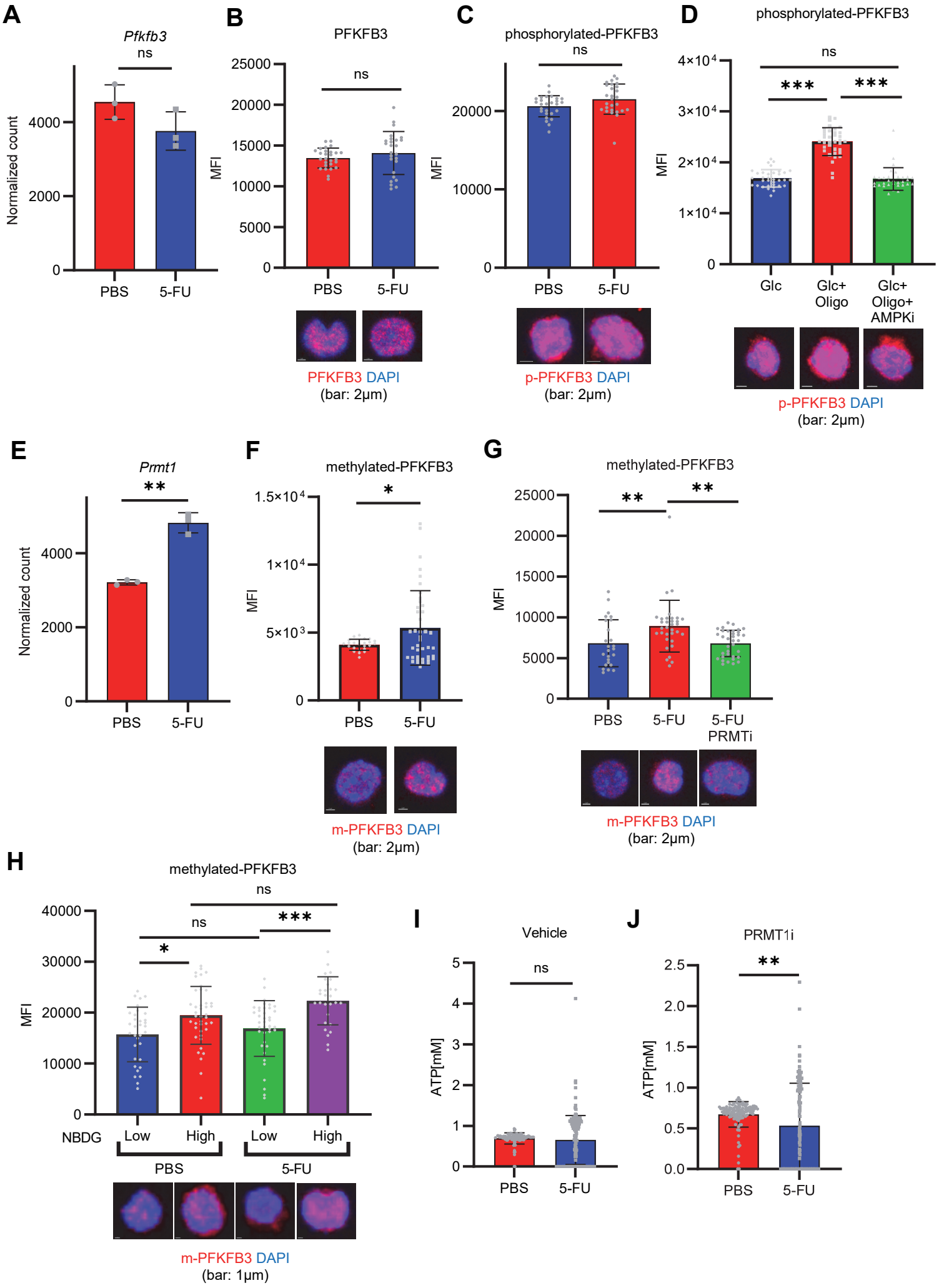
A
Pfkfb3
ns
Normalized count
4000
2000
0
PBS
5-FU
B
PFKFB3
ns
MFI
25000
20000
15000
10000
5000
0
PBS
5-FU
PFKFB3 DAPI
(bar: 2μm)
C
phosphorylated-PFKFB3
ns
MFI
20000
10000
0
PBS
5-FU
p-PFKFB3 DAPI
(bar: 2μm)
D
phosphorylated-PFKFB3
ns
***
***
MFI
4×10⁴
3×10⁴
2×10⁴
1×10⁴
0
Glc
Glc+ Oligo
Glc+ Oligo+ AMPKi
p-PFKFB3 DAPI
(bar: 2μm)
E
Prmt1
**
Normalized count
4000
2000
0
PBS
5-FU
F
methylated-PFKFB3
*
MFI
1.5×10⁴
1×10⁴
5×10³
0
PBS
5-FU
m-PFKFB3 DAPI
(bar: 2μm)
G
methylated-PFKFB3
**
**
MFI
25000
20000
15000
10000
5000
0
PBS
5-FU
5-FU PRMTi
m-PFKFB3 DAPI
(bar: 2μm)
H
methylated-PFKFB3
ns
ns
***
*
MFI
40000
30000
20000
10000
0
NBDG
Low
High
Low
High
PBS
5-FU
m-PFKFB3 DAPI
(bar: 1μm)
I
Vehicle
ns
ATP[mM]
5
4
3
2
1
0
PBS
5-FU
J
PRMT1i
**
ATP[mM]
2.5
2.0
1.5
1.0
0.5
0.0
PBS
5-FU

Figure 7

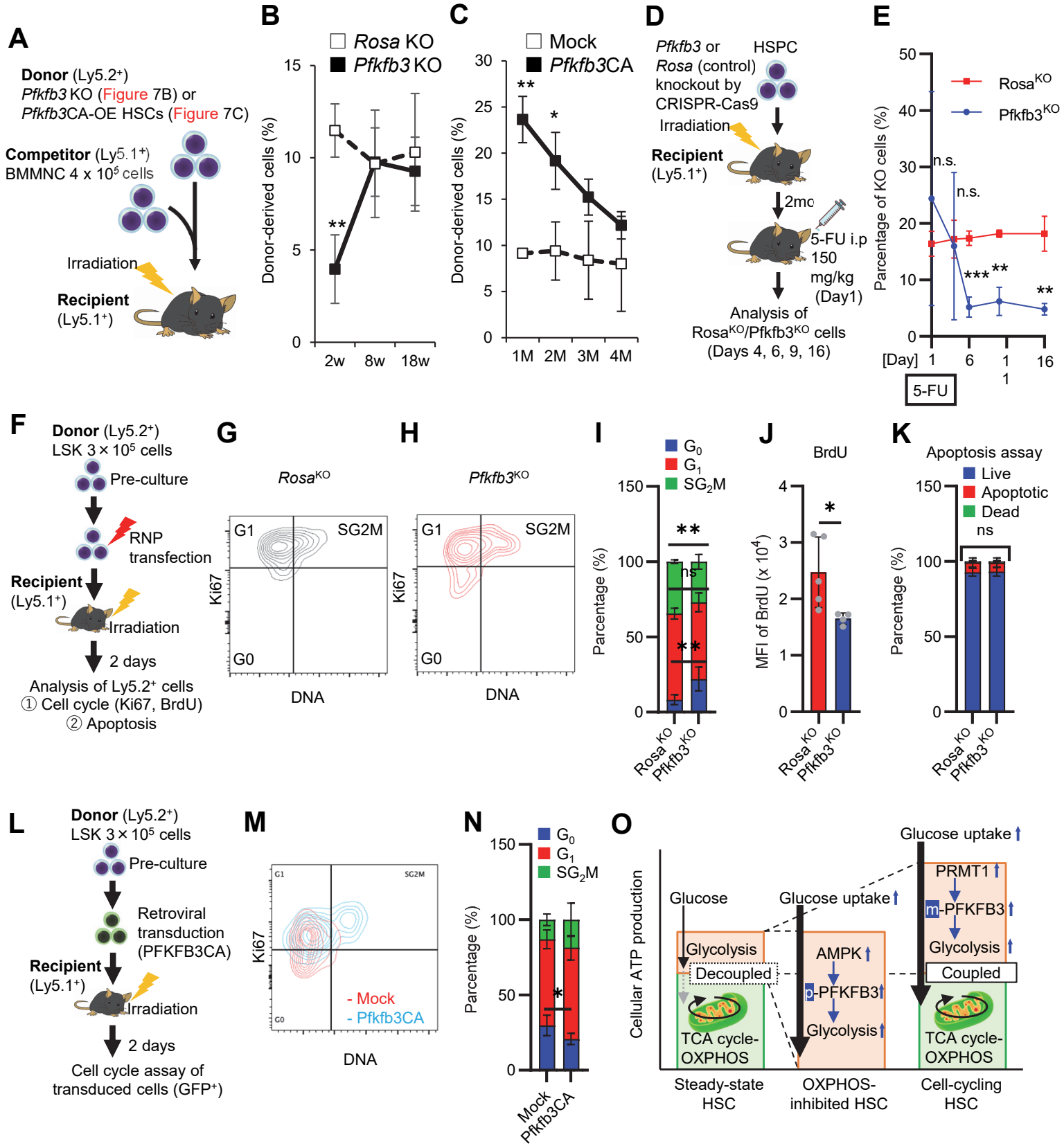
A
Donor (Ly5.2+)
Pfkfb3 KO (Figure 7B) or
Pfkfb3CA-OE HSCs (Figure 7C)
Competitor (Ly5.1+)
BMMNC 4 x 10^5 cells
Irradiation
Recipient
(Ly5.1+)
B
Rosa KO
Pfkfb3 KO
Donor-derived cells (%)
2w
8w
18w
C
Mock
Pfkfb3CA
Donor-derived cells (%)
1M
2M
3M
4M
D
Pfkfb3 or
Rosa (control)
knockout by
CRISPR-Cas9
HSPC
Irradiation
Recipient
(Ly5.1+)
2mo
5-FU i.p
150
mg/kg
(Day1)
Analysis of
RosaKO/Pfkfb3KO cells
(Days 4, 6, 9, 16)
E
RosaKO
Pfkfb3KO
Parcentage of KO cells (%)
n.s.
n.s.
[Day]
5-FU
F
Donor (Ly5.2+)
LSK 3 × 10^5 cells
Pre-culture
RNP
transfection
Recipient
(Ly5.1+)
Irradiation
2 days
Analysis of Ly5.2+ cells
① Cell cycle (Ki67, BrdU)
② Apoptosis
G
RosaKO
G1
SG2M
G0
Ki67
DNA
H
PfkfbKO
G1
SG2M
G0
Ki67
DNA
I
G0
G1
SG2M
Parcentage (%)
ns
RosaKO
Pfkfb3KO
J
BrdU
MFI of BrdU (x 10^4)
RosaKO
Pfkfb3KO
K
Apoptosis assay
Live
Apoptotic
Dead
ns
Parcentage (%)
RosaKO
Pfkfb3KO
L
Donor (Ly5.2+)
LSK 3 × 10^5 cells
Pre-culture
Retroviral
transduction
(PFKFB3CA)
Recipient
(Ly5.1+)
Irradiation
2 days
Cell cycle assay of
transduced cells (GFP+)
M
G1
SG2M
G0
Ki67
DNA
- Mock
- Pfkfb3CA
N
G0
G1
SG2M
Parcentage (%)
Mock
Pfkfb3CA
O
Cellular ATP production
Glucose
Glycolysis
Decoupled
TCA cycle-
OXPHOS
Steady-state
HSC
Glucose uptake
AMPK
p-PFKFB3
Glycolysis
OXPHOS-
inhibited HSC
Glucose uptake
PRMT1
m-PFKFB3
Glycolysis
Coupled
TCA cycle-
OXPHOS
Cell-cycling
HSC